京都大学防災研究所年報 第 54 号 B 平成 23 年 6 月
Annuals of Disas. Prev. Res. Inst., Kyoto Univ., No. 54 B, 2011

Assessment of Glacial Hazards in Rolwaling Valley of Nepal and Numerical Approach to Predict Glacial Lake Outburst Flood

Badri Bhakta SHRESTHA, Hajime NAKAGAWA, Kenji KAWAIKE,
Yasuyuki BABA and Hao ZHANG

Synopsis

In recent years climate change and retreating glaciers constitute a major hazard in the Himalaya of South Asia or glacier regions of the world. Glacial lakes are rapidly developing or increasing due to climate change, which may cause the outburst of the lake. The outburst discharge from the glacial lake can cause catastrophic flooding and disasters in downstream area. Therefore, it is necessary to investigate the impact of climate change on glacial lakes and to understand the behavior of the glacial lakes. In this study, the field assessment of Tsho Rolpa Glacial Lake in the Himalaya of Nepal has been presented and the impact of climate change on this glacial lake has been discussed. The Tsho Rolpa Glacial Lake is the largest and most potentially dangerous glacial lake in Nepal. A numerical model has been also developed for computing the characteristics of glacial lake outburst due to moraine dam failure by seepage and water overtopping. The simulated results are compared with the experimental results.

Keywords: GLOF, impact of climate change, moraine dam failure, numerical analysis, Tsho Rolpa Glacial Lake, glacial hazard assessment

1. Introduction

Floods and debris flows are frequently occurred in the Himalaya of South Asia or glacier regions of the world in recent years due to glacial lakes outburst (Shrestha et al., 2010a, 2010b). The Himalayan glaciers are rapidly melting due to climate change, which results the formation or rapid development of the glacial lakes (Osti and Egashira, 2009). The rapid development of glacial lake may cause the outburst of the lake at any time.

Glacial Lake Outburst Floods (GLOFs) typically occur by lake water overflowing and eroding the moraine dam. A trigger mechanism such as displacement wave from an ice or rock avalanche, or disintegrating ice-core within the dam, or seepage/piping in the dam, or water level rising is normally required (Richardson and Reynolds, 2000). The moraine dams are comparatively weak and can breach suddenly, leading to the sudden discharge of huge volumes of water and debris (Bajracharya et al., 2006). The GLOF events can cause catastrophic flooding in downstream areas, with serious damage to life and property (Yamada, 1998; Bajracharya et al., 2006, 2007a; Wang et al., 2008). Therefore, to avoid or minimize loss of life and property, there is a pressing need mechanism approaches to investigate the outburst of glacial lakes and its downstream impacts.

The characteristics of glacial lakes and their outburst are poorly understood. However, some attempts have been carried out on the investigation of the impact of climate change on the Himalayan glaciers (Bajracharya et al., 2006; Bajracharya, 2010) and on the characteristics of the GLOF events (Bajracharya et al., 2007b; Wang et al., 2008; Osti and Egashira, 2009; Shrestha et al., 2010c, 2010d).

The Tsho Rolpa Glacial Lake is the largest and

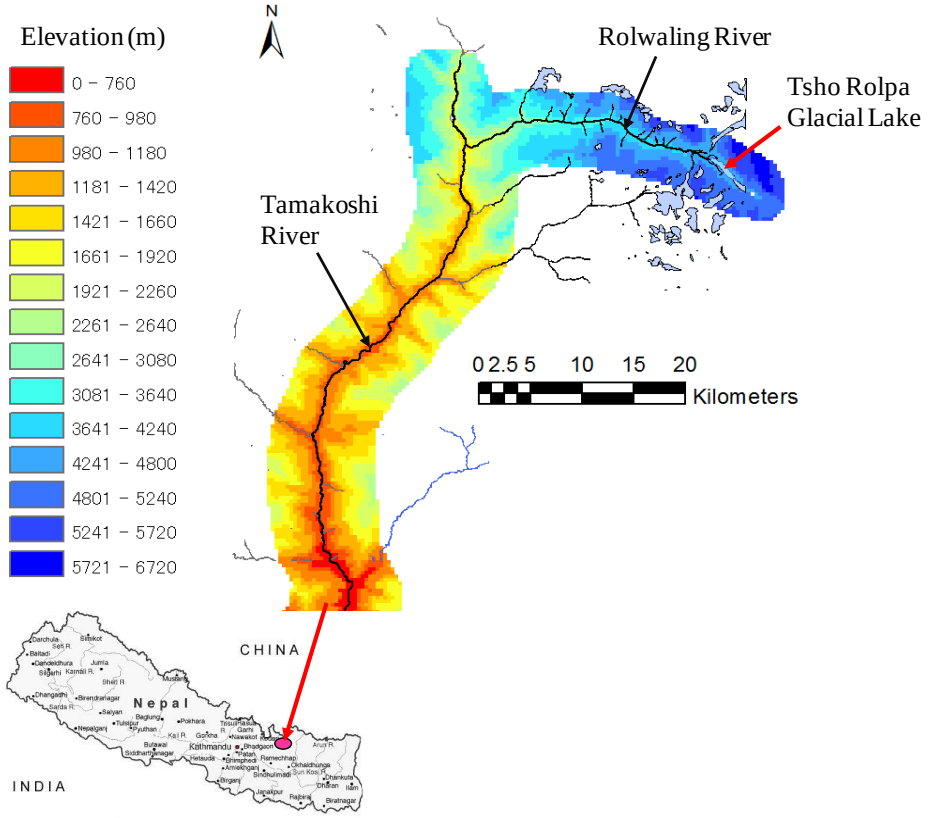

Fig. 1 Location of Tsho Rolpa Glacial Lake and digital elevation model of river valley

most potentially dangerous glacial lake in Nepal. Thus, the investigation of the downstream impacts of the potential GLOF events from the Tsho Rolpa Glacial Lake is necessary. In this study, the field assessment of Tsho Rolpa Glacial Lake in Rolwaling valley of Nepal has been presented and the impact of climate change on glacial lake has been also analyzed. A numerical model has been also developed to compute the characteristics of glacial lake outburst due to moraine dam failure by seepage and water overtopping. To compute the pore-water pressure in the moraine dam and slope stability of the dam, a seepage flow model and a slope stability model are incorporated into a numerical model of flow and dam surface erosion. The simulated results are compared with the results obtained from the hydraulic model experiments.

2. Field Assessment and Impact of Climate Change on Tsho Rolpa Glacial Lake

Due to impact of global climate change, glaciers in the Himalaya are rapidly melting in recent years. Global warming has accelerated glacial retreat, which results the formation or expansion of glacial lakes and constitutes a major hazards in the Himalaya. The warming in the Himalayas in last three decades has been between 0.15˚C-0.6˚C per decade (Bajracharya, 2010). About 2,323 glacial lakes are identified in Nepal, out of which 17 lakes are identified as potentially dangerous (Bajracharya, 2010). Tsho Rolpa Glacial Lake is largest and most potentially dangerous glacial lake in Nepal. The Tsho Rolpa Glacial Lake (27°51'N, 86°29'E) is located in the Rolwaling valley of Nepal at an elevation of 4555m (measured at the field). Fig. 1 shows the location of the Tsho Rolpa Glacial Lake and Digital Elevation Model (DEM) of the study area. A DEM is derived from digital contour data prepared by the Survey Department of Nepal. The lake has begun to develop in 1950s due to glacier retreating or melting. The trakarding glacier above the lake is retreating at a rate of over 20 meters a year due to rising temperatures. The lake is 3.23km long and 0.5km wide, and 1.76km^2 surface area and contained 86 million m^3 water (Mool, 2010). The lake

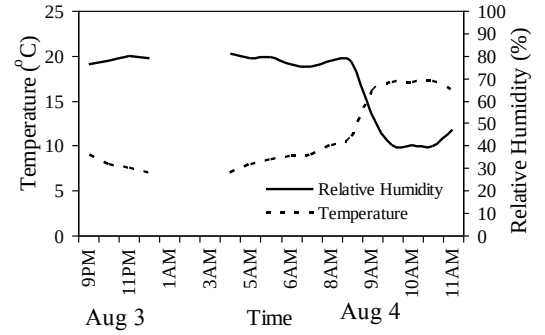

(a) At lake

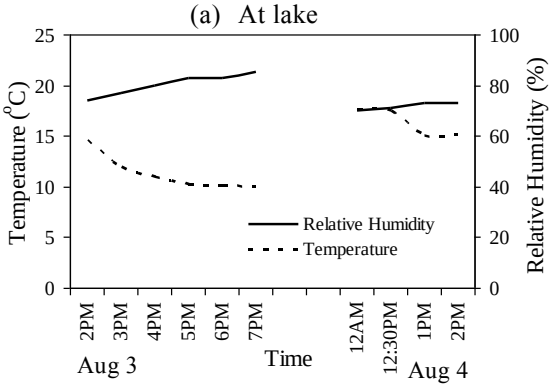

(b) At Naa Village (3.2km downstream)

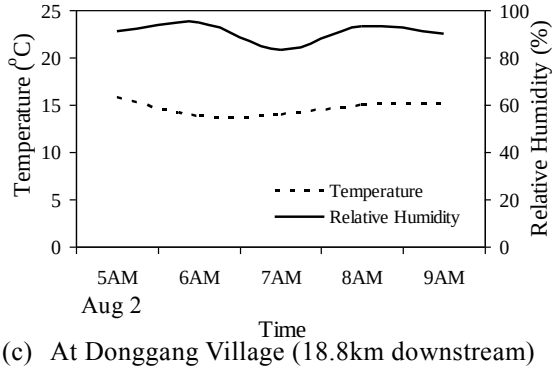

(c) At Donggang Village (18.8km downstream)

Fig. 2 Measured temperatures and relative humidity at the lake and downstream villages (in 2010)

is considered one of the most dangerous glacial lakes in Nepal. During the field visit, it was observed that the maximum temperature at the lake is about 17.2°C at sunny time in the month of August, 2010. Fig. 2 shows the measured temperature and the relative humidity at the lake and at the downstream villages. Fig. 3 shows the measured air pressure, temperature and relative humidity along the downstream river valley from the lake and their relationships. The air pressure at the lake is about 591hpa. The measure relative humidity at the lake is ranging from 38-81% depending on temperature variations. The temperature at the lake is low during mid night and the relative humidity becomes higher at that time. Fig. 4 shows the trend of temperature and precipitation change at the Tsho Rolpa Glacial

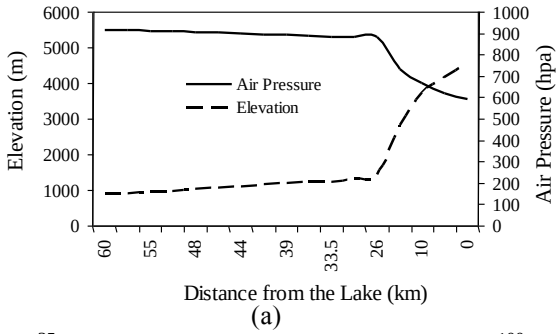

(a)

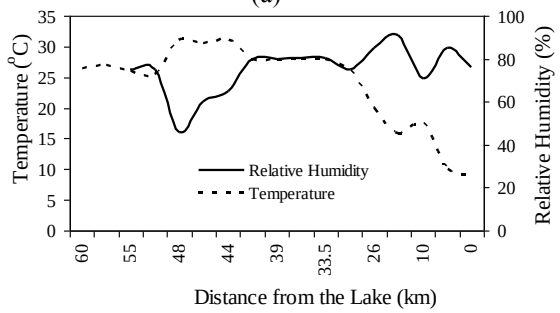

(b)

Fig. 3 (a) Relationship between air pressure and altitude along the downstream river valley from the lake, (b) Relationship between temperature and relative humidity along the river valley (in 2010)

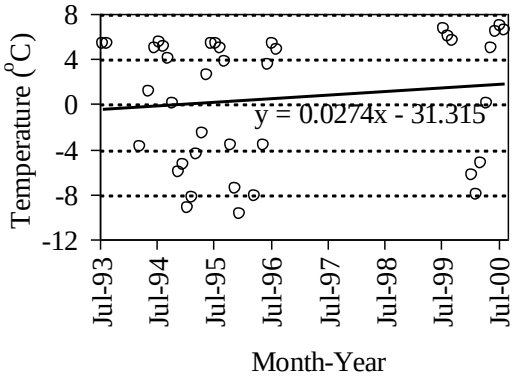

(a) Trend of temperature change

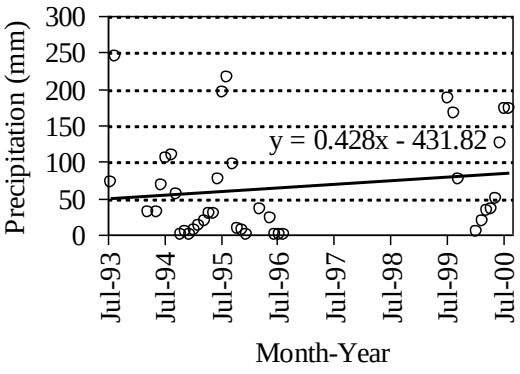

(b) Trend of precipitation change

Fig. 4 Trend of temperature and precipitation changes at Tsho Rolpa Glacial Lake (Data Source: Department of Hydrology and Metrology (DHM), Nepal)

Lake. Both the temperature and the precipitation are increasing in trend.

The Tsho Rolpa Glacial Lake has increased by five times since 1960. Figs. 5 and 6 show the growth of the lake and the trend of lake area expansion, respectively. The lake size is rapidly increasing in trend. However, after the construction of open channel for lake discharge outflow in 2000, the surface lake area is almost constant. The lake water level was reduced by 3m due to construction of channel. But the lake is still in most potentially dangerous. Fig. 7 shows the variations of different characteristics of the Tsho Rolpa Glacial Lake. The lake is retained by a natural moraine dam. The inner and outer slopes of the end moraine dam vary from 15-25^o and 20-40^o, respectively. The inner slopes of the lateral moraines damming the sides of the lake are very steep (25-90^o).

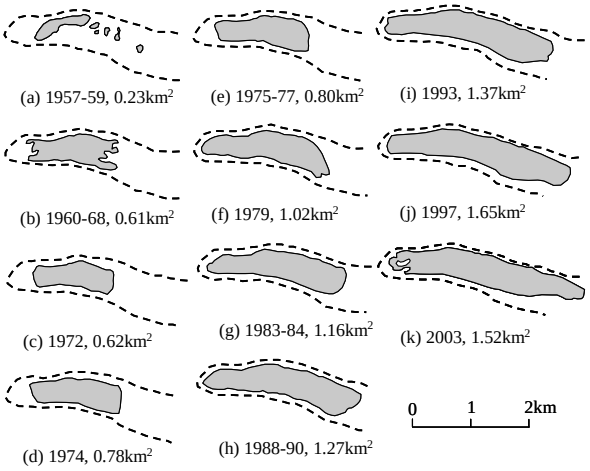

Fig. 5 Growth of Tsho Rolpa Glacial Lake in Rolwaling valley, Nepal (Modified from Horstmann, 2004)

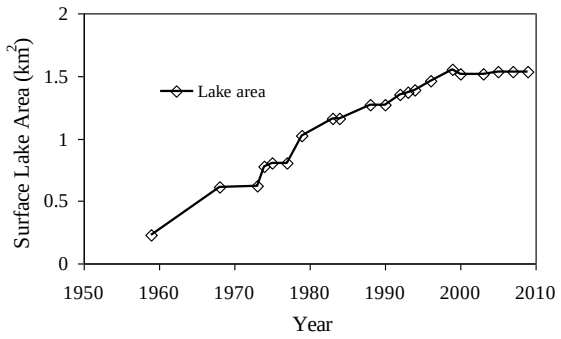

Fig. 6 Trend of lake area expansion (Source: various literatures)

Fig. 8 shows the upstream view of the Tsho Rolpa Glacial Lake and the steeply hanging glaciers at the right side of the lake. If such hanging glaciers fall into the lake may generate the wave in the lake, which may overtop the dam and erode it. Thus, this lake can be outburst by glacier mass fall into the lake. This lake can be outburst also due to seepage and sudden collapse of the moraine dam caused by melting of ice core inside the dam. The Himalayan temperature is increasing due to climate change, which causes the melting of ice core inside the dam and sudden collapse of dam may occur. Fig. 9a shows the trakarding glacier at the end of the lake, which is melting at the rate of more than 20m per year. Fig. 9b shows the constructed lake outlet channel at the end of the moraine dam. The glaciers are in rapidly melting, which may cause the outburst of the lake at any time. The outburst of the lake causes the catastrophic flooding and disasters in downstream area. Fig. 10 shows the end of moraine dam and lake water outflow. Fig. 11 shows

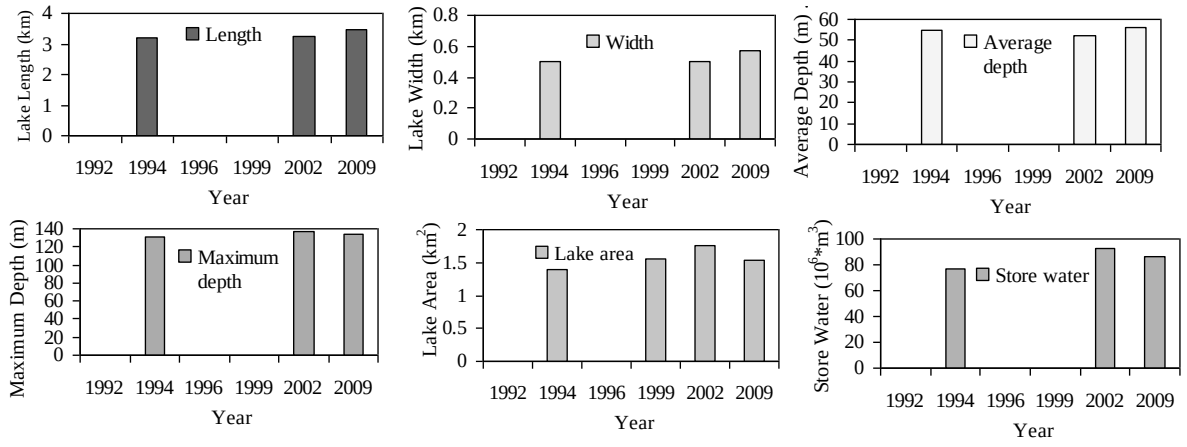

Fig. 7 Variations of different characteristics of Tsho Rolpa Glacial Lake (Sources: DHM and unpublished report of International Center for Integrated Mountain Development (ICIMOD), 2010)

Fig. 8 Tsho Rolpa Glacial Lake and steeply hanging glaciers at right side of the lake (upstream end upward) (Photograph by: Badri Bhakta Shrestha, August 2010)

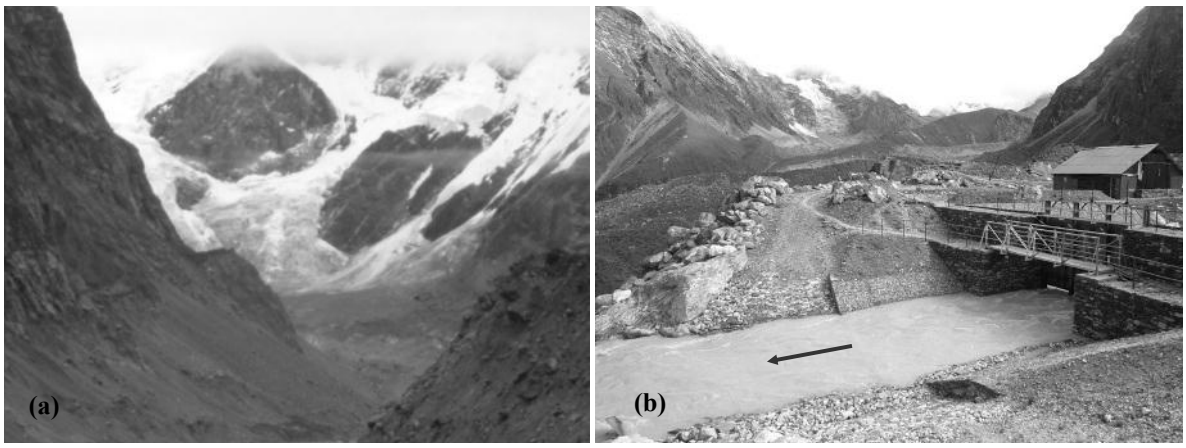

Fig. 9 (a) Trakarding glacier at the upstream end of the lake, (b) Lake outlet open channel constructed at the end of moraine dam (Photograph by: Badri Bhakta Shrestha, August 2010)

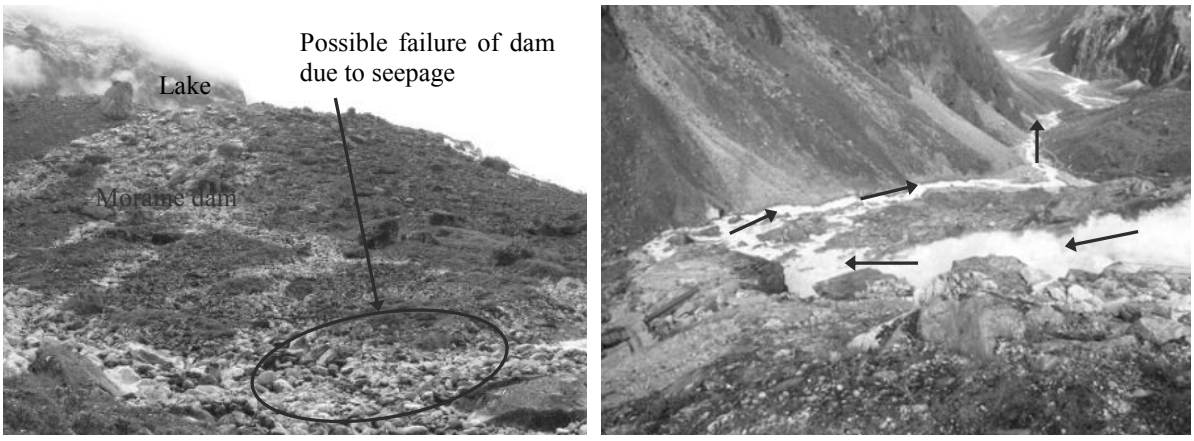

Fig. 10 End of moraine dam and lake water outflow (Photograph by: Badri Bhakta Shrestha, August 2010)

the outlet channel approaching from lake. The open channel length, width and depth are about 70m, 6.4m and 4.2m, respectively. The width of gate opening is about 3m and the gate can controlled outflow discharge 15-30m^3/sec. Fig. 12 shows the top of end moraine and sediment composition. The moraine consists of large boulders and rocks. Some of the rocks are more than two meters in diameter. The matrix of the moraine is sand and smaller boulders and cobbles. At the surface of the end

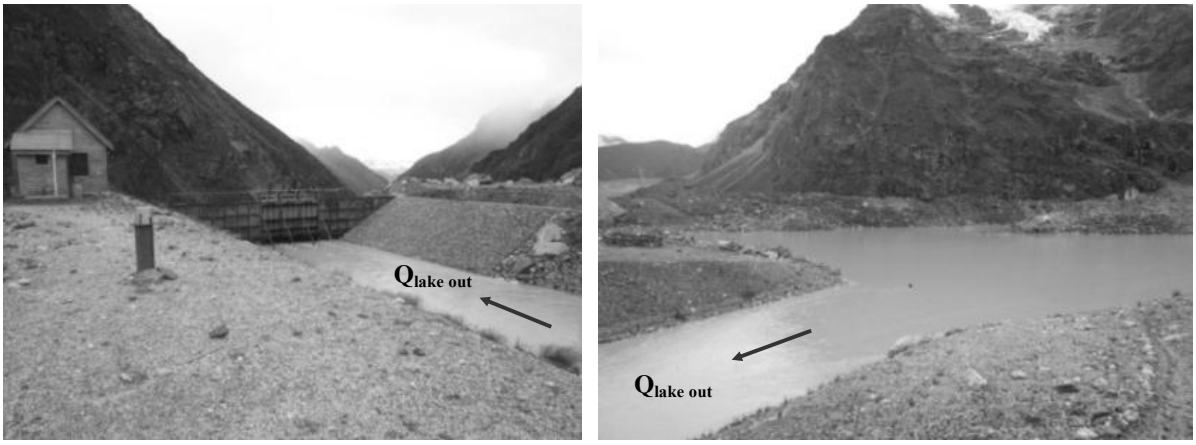

Fig. 11 Outlet channel from lake (70m long) (Photograph by: Badri Bhakta Shrestha, August 2010)

Fig. 12 Top of end moraine and sediment composition (Photograph by: Badri Bhakta Shrestha, August 2010)

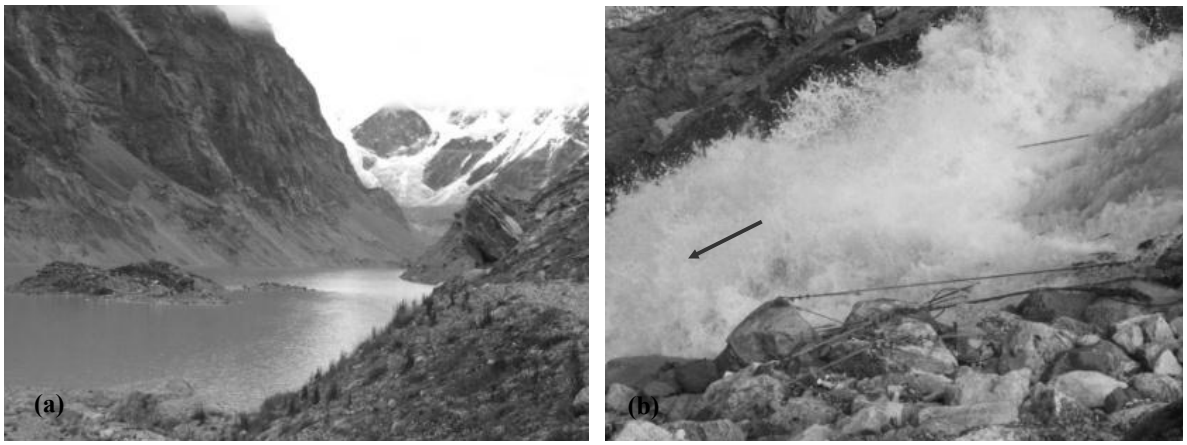

Fig. 13 (a) Lateral moraines of the lake and vertical cliff at right side, (b) Lake outflow discharge and rock anchoring at moraine dam slope (Photograph by: Badri Bhakta Shrestha, August 2010)

moraine there is less fine sediments than boulders and cobbles (WECS, 1993). Fig. 13a shows the lateral moraines of the lake and steep vertical cliff at right side of the lake where many glaciers are in steeply hanging. Fig. 13b shows the outflow discharge from the lake and rock anchoring at moraine dam slope to prevent erosion of the dam surface from outflow discharge of the lake.

GLOF typically occurs due to moraine dam failure caused by seepage and lake water overtopping and eroding the dam. The moraine dams are comparatively weak and can breach suddenly, leading to the sudden discharge of huge volumes of water and debris. If the moraine dam of Tsho Rolpa Glacial Lake will breach, the resulting flood from the lake would cause serious damage for

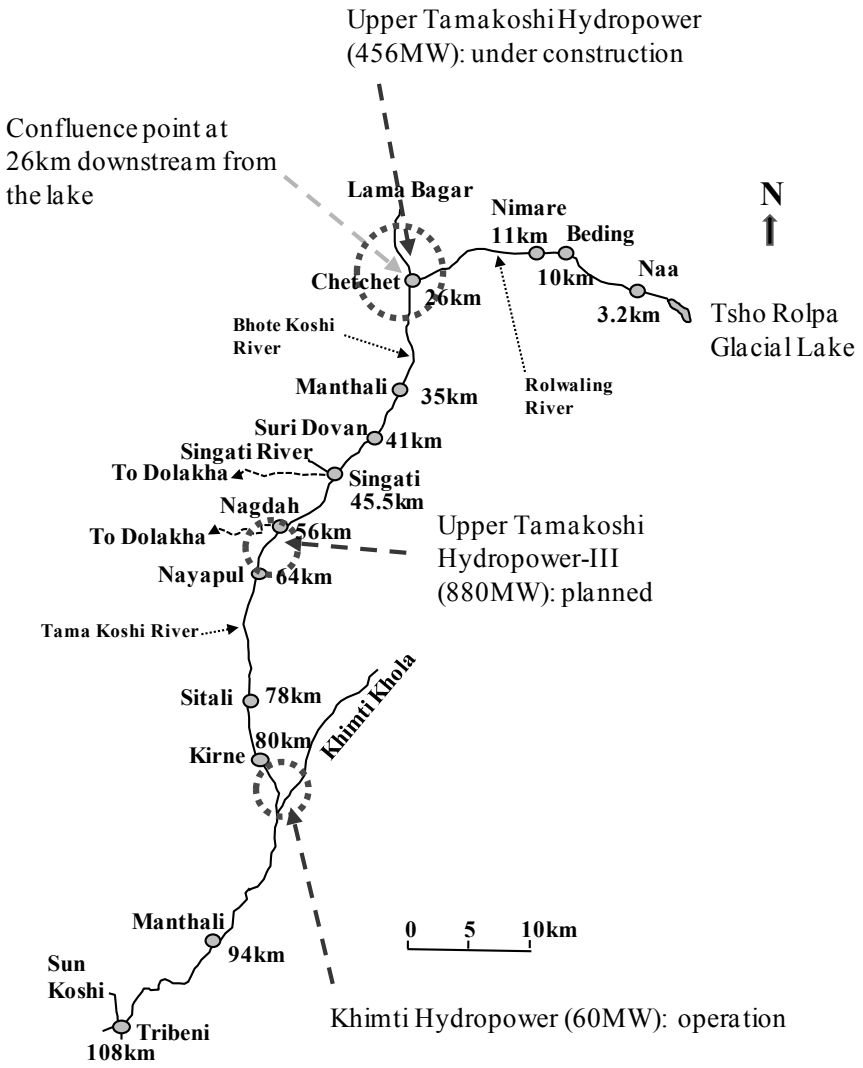

Fig. 14 Downstream main settlement villages along Rolwaling and Bhotekoshi/Tamakoshi Rivers

100km or more downstream, threatening many people, two hydroelectric projects (one is in operation phase, i.e., Khimti Hydropower of 60MW and another is in under construction phase, i.e., Upper Tamakoshi Hydroelectric Project of 456MW) and other infrastructures. Therefore, the countermeasures are necessary to reduce the extent of damage by the probable flood due to GLOF event. Fig. 14 shows the main settlement areas along the Rolwaling and Tamakoshi Rivers downstream from the lake. Fig. 15 shows the longitudinal downstream river profile from the lake. The main drainage in the Rolwaling valley is Rolwaling River originating from glacier melts and Tsho Rolpa Glacial Lake (Fig. 14). Rolwaling River joins with Bhote-Tamakoshi River near Chetchet at about 26km downstream from the lake. The average

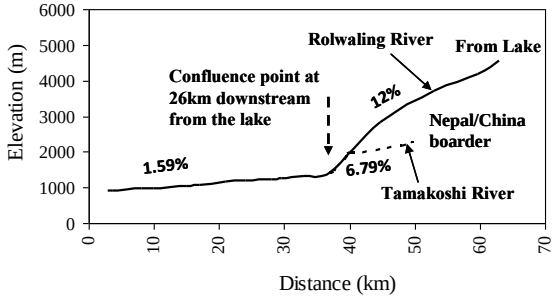

Fig. 15 Longitudinal river bed profile of Tamakoshi and Rolwaling rivers

slope of the Rolwaling River is about 12% and the average slope of the Tamakoshi River downstream from the confluence point is about 1.59%. Fig. 16a shows the Rolwaling River near Naa village and Fig. 16b shows the photograph of Naa village, which is situated at an altitude of 4100m at a distance 3.2km downstream from the lake. Fig. 17 shows the

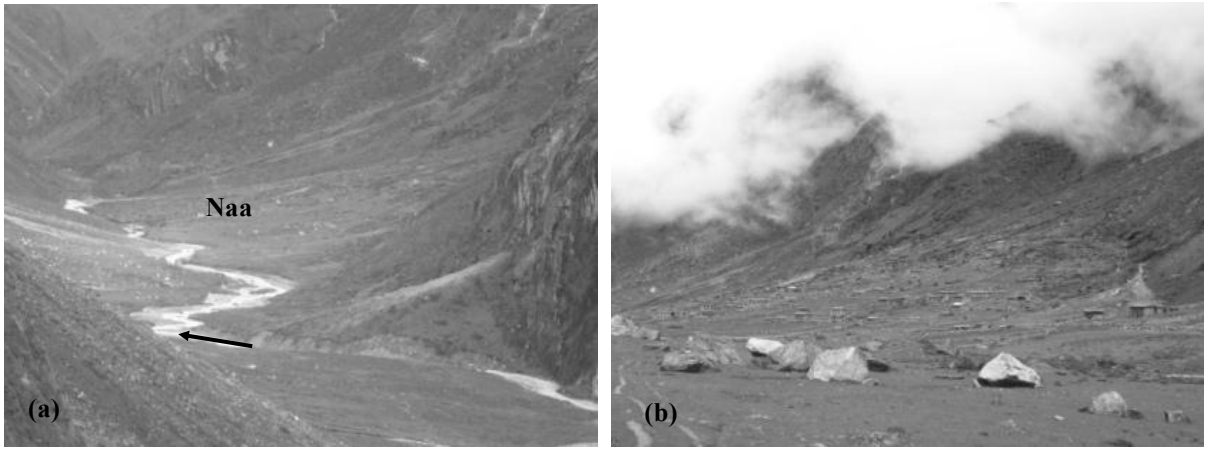

Fig. 16 (a) Photo of Rolwaling River near Naa village from the lake, (b) Naa village 3.2km downstream from the lake (Photograph by: Badri Bhakta Shrestha, August 2010)

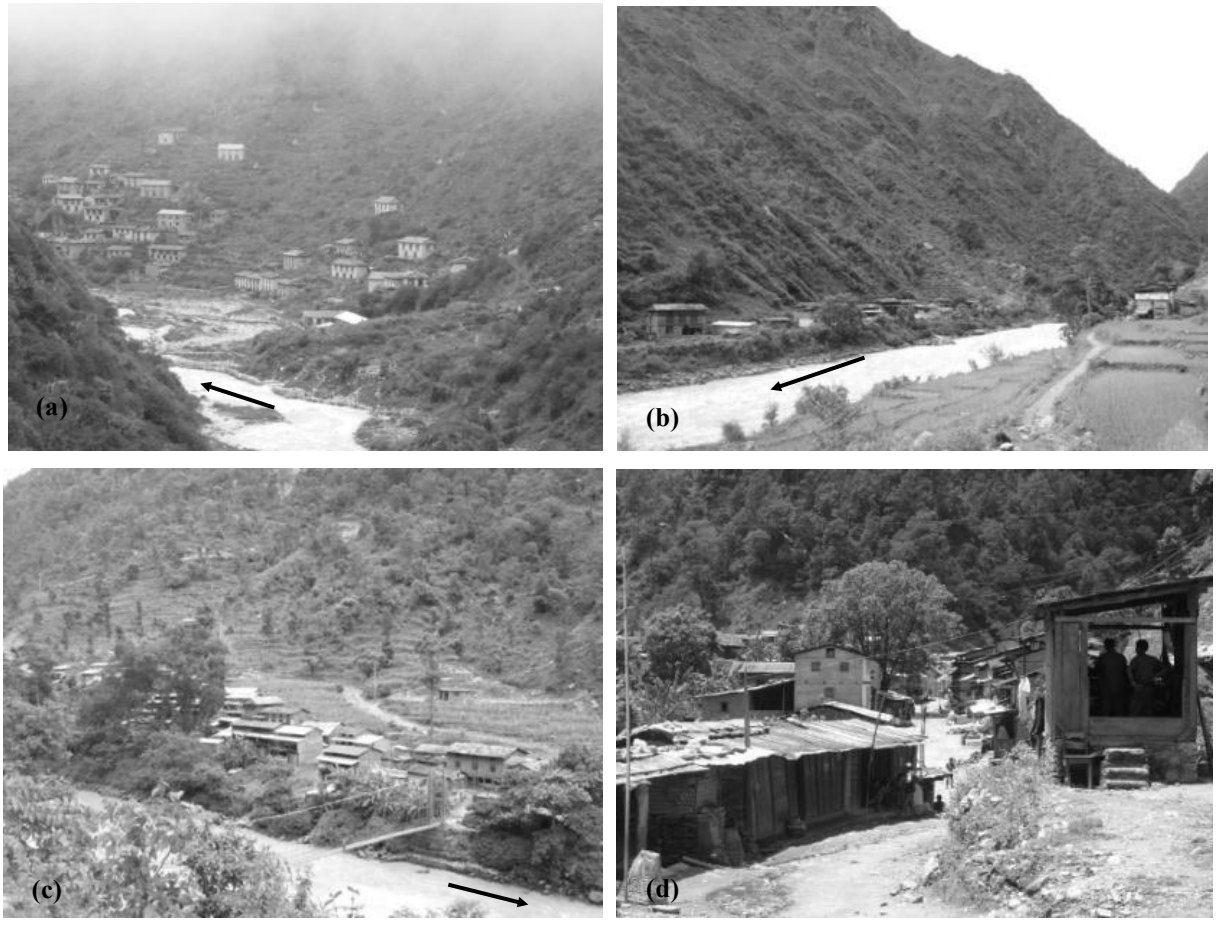

Fig. 17 Villages along downstream river valley (a) Beding village (10km downstream), (b) Jagat village (33.8km downstream), (c) Bhorle village (43.3km downstream), and (d) Singati village (main market center of this area) (45.5km downstream) (Photograph by: Badri Bhakta Shrestha, August 2010)

photographs of some villages situated at downstream river valley.

Fig. 18 shows the installed sirens for early warning system at near downstream end of moraine dam and at Gongar village. In 1998, early warning systems were installed at 19 stations in main settlement area along Rolwaling and Tamakoshi Rivers. These automated early warning systems were installed with financial support from the World Bank (Matambo and Shrestha, 2011). But

Fig. 18 (a) Siren at near downstream end of moraine dam, (b) Siren at Gongar village (30.4km downstream) (Photograph by: Badri Bhakta Shrestha, August 2010)

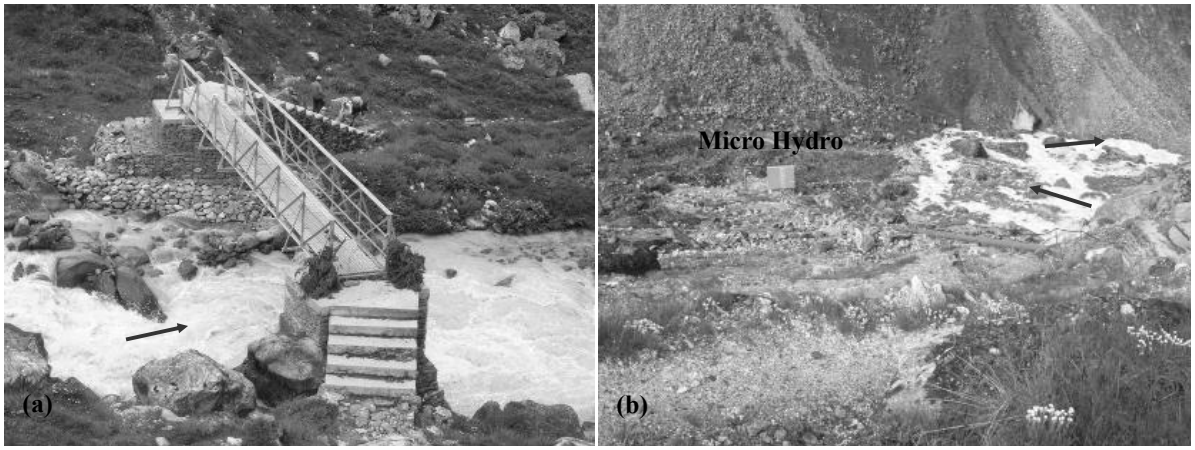

Fig. 19 (a) Steel truss bridge just downstream of moraine dam at Rolwaling River, (b) 15kw micro hydro operation from lake outflow discharge (Photograph by: Badri Bhakta Shrestha, August 2010)

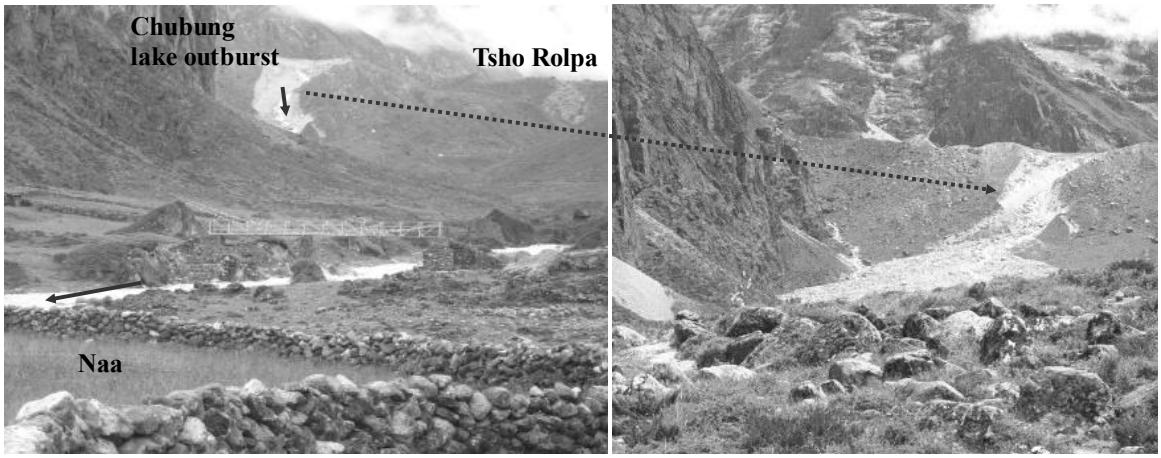

Fig. 20 Chubung glacial lake outburst on 12 July, 1991, close to Tsho Rolpa Glacial Lake (Photograph by: Badri Bhakta Shrestha, August 2010)

currently these systems are not in operation. Fig. 19a shows the steel truss bridge just downstream of moraine dam and Fig. 19b shows the photograph of micro hydro plant (15kw) at moraine dam of Tsho Rolpa Glacial Lake which is in operation since 2003 by using the lake water flowing out the open channel of the lake outlet.

Fig. 20 shows the moraine dam breaching of

Chubung Glacial Lake on 12 July 1991, which is close to Tsho Rolpa Glacial Lake. The Chubung Lake was outburst due to falling of ice avalanche into the lake caused by temperature rise in the area. The breaching depth and width of moraine dam of Chubung lake outburst are about 15m and 20m, respectively (Reynolds, 1999). The GLOF event from Chubung Lake possibly was caused by chain outburst of several small ponds (Bajracharya, 2008). The flood from Chubung glacial lake outburst killed some livestock and destroyed one bridge in Naa village. This flood also killed one person and destroyed several houses, three flour mills and several potato fields in Beding village (Reynolds, 1999, Bajracharya, 2008). The potential outburst flood from Tsho Rolpa Glacial Lake can be hundreds time higher than flood from Chubung lake outburst. More than 80 million m^3 of water can be drained from Tsho Rolpa Glacial Lake. The resulting potential outburst flood from Tsho Rolpa Glacial Lake can cause greatest property damage and loss of life. Therefore, the preparation of flood inundation or hazard maps and countermeasures with early warning systems and evacuation planning are very necessary to minimize loss of life and property damage from potential outburst flood from Tsho Rolpa Glacial Lake.

3. Analysis of Lake Outflow Discharge

The Rolwaling River is the main drainage in the Rolwaling valley, which is mainly originating from Tsho Rolpa Glacial Lake and glacier melts (Fig. 15). The total catchment area of the Rolwaling valley is 307km^2. The catchment areas up to the Tsho Rolpa Glacial Lake outlet point, up to Naa village and up to Beding village are 79km^2, 160km^2 and 197km^2, respectively (WECS, 1993). Several tributary streams join Rolwaling River. However, Tshu Rawa stream originating from the outlet of Tsho Rolpa Glacial Lake is considered as one of the main source of the Rolwaling River. The outflow discharge from the Tsho Rolpa Glacial Lake is mainly due to accumulation of melting water from the glaciers and the precipitation in the watershed in the lake and the outflow discharge from the lake flows through the channel at the end moraine dam until the lake frozen. The annual amount of lake

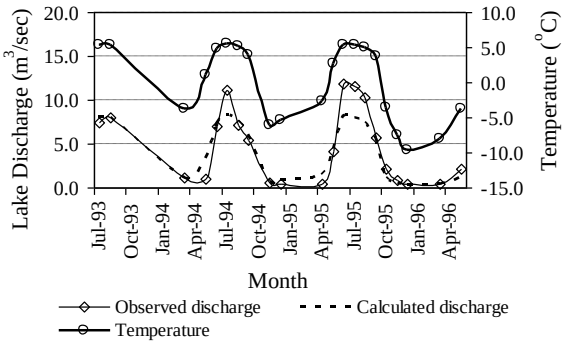

Fig. 21 Relation of temperature and lake outflow discharge at Tsho Rolpa Glacial Lake (Observed data source: DHM, Nepal)

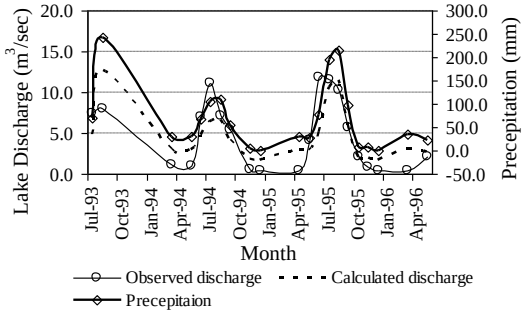

Fig. 22 Relation of precipitation and lake outflow discharge at Tsho Rolpa Glacial Lake (Observed data source: DHM, Nepal)

discharge is about 95.5 million m^3 and the annual average discharge is 3.03m^3/sec (Mool et al., 2001). From the regression analysis, the relationship between monthly average discharge from the lake and the temperature at the lake is obtained as

$$Q_{lake} = 2.5496 \times e^{(0.214 \times T)} \quad (1)$$

where Q_{lake} is the outflow discharge from the lake in m^3/sec and T is the average temperature at the lake in ^oC. Fig. 21 shows the relationship of average temperature at the lake and the monthly average discharge from the lake. The calculated discharge based on the regression analysis of the observed data is also shown in the figure. The maximum outflow discharge from the lake is in the month of July or August when the temperature at the lake is higher. The high outflow period of the average monthly discharge from the lake is in between May to October. The relationships of the average monthly lake outflow discharge with precipitation and with both temperature and precipitation respectively, are expressed as

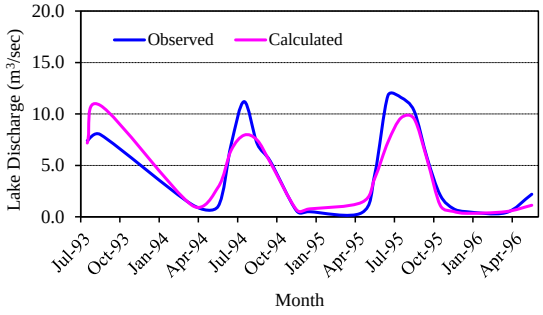

Fig. 23 Observed and calculated monthly average discharge from the lake using Eq. (3) (Observed data source: DHM, Nepal)

$$Q_{lake} = 1.6507 + 0.0453 \times P \quad (2)$$

$$Q_{lake} = 2.1533 \times e^{(0.0025 \times P + 0.19 \times T)} \quad (3)$$

where P is the monthly precipitation in mm. Fig. 22 shows the relationship of monthly average discharge with monthly precipitation. The calculated monthly lake discharge by using the relationship of both the precipitation and temperature (Eq. (3)) are shown in Fig. 23.

The outflow discharge from the lake flows to Rolwaling River and it joins with Bhote-Tamakoshi River at about 26km downstream from the lake in Chetchet. Fig. 24 shows the observed five years period monthly average discharge and maximum discharge at Busti station about 63km downstream from the lake. The gauging station at Busti Station in Tamakoshi River has a catchment area of 2700km^2 and it is located at an altitude of 849m. The variations of monthly average discharge during monsoon season at Busti station are shown in Fig. 25. The trend of maximum yearly average discharge is shown in Fig. 26 and the maximum discharge is increasing in trend that may be due to higher rate of glaciers melt and increase in precipitation caused by climate change.

4. Numerical Approach to Analyze the Glacial Lake Outburst Flood

Numerical model is a very useful tool for planning efficient countermeasures against GLOF events and to prepare necessary information about disasters for raising awareness and preparedness of GLOF disasters to society. Thus, the development

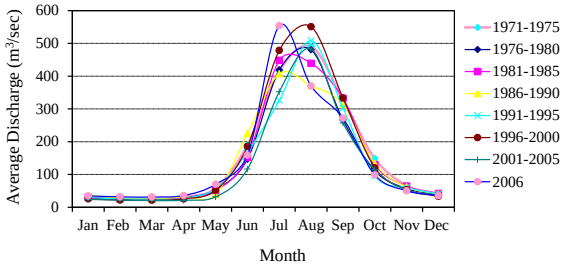

(a) Average discharge

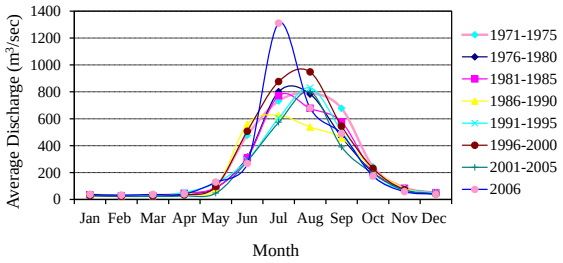

(b) Maximum discharge

Fig. 24 Observed five years period monthly discharge from 1971 to 2006 at Busti station (63km downstream from the lake) (Data source: DHM, 2008)

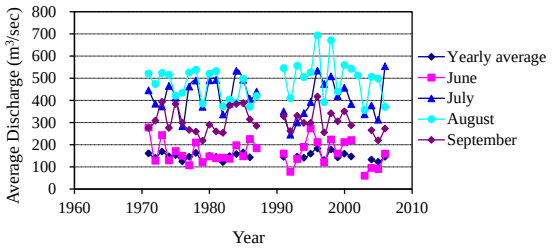

Fig. 25 Observed monthly average discharge of 1971 to 2006 in monsoon season at Busti station (Data source: DHM, 2008)

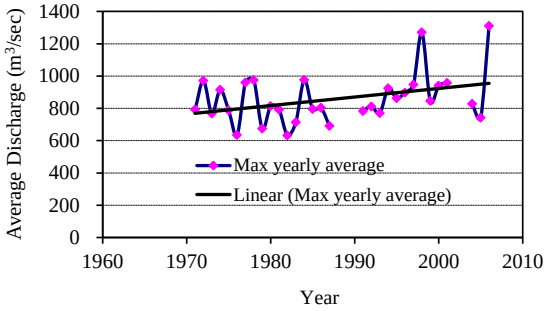

Fig. 26 Trend of observed maximum yearly average discharge from 1971 to 2006 at Busti station (Data source: DHM, 2008)

of numerical model is very necessary for implementing structural as well as non-structural countermeasures. The previous researches on GLOF are mainly focused on satellite observations, accounts of past events and preventive measures. The studies of GLOF events and their downstream flooding are very limited. The failure mechanism

and erosion process of moraine dam are still not thoroughly understood. However, some empirical relationships and also physically based models are established to compute the characteristics of breaching of moraine dammed glacial lake. The empirical relationships are derived to predict the peak discharge of glacial lake outburst with relations of lake volume, depth and area (Evans, 1986; Costa and Schuster, 1988; Clague and Evans, 2000; Cenderelli and Wohl, 2001; Huggel et al., 2002, 2004; Dwivedi, 2005; Shrestha et al., 2010a). These relationships are mainly related with lake volume only and are derived from the limited number of recorded data. However, the peak discharge is depended on various factors such as dam characteristics, failure mechanisms, sediment properties, erosion mechanism of moraine dam and others, which are not included in the empirical relationships.

Physically based models such as NWS-DAMBRK (Fread, 1988) and NWS-BREACH (Fread, 1991) are commonly used to predict the outflow hydrograph of glacial lake outburst (Bajracharya et al., 2007b; Wang et al., 2008; Shrestha et al., 2010). Furthermore, HEC-RAS dam breach model (U.S. Corps of Engineers, 2002) is also employed by Osti and Egashira (2009) to predict the outflow hydrograph of glacial lake outburst. The limitation of these models is that these models do not consider the actual mechanism of dam surface slope failure and headcut and lateral dam surface erosion. In addition, the downstream flooding or impact of some GLOF events is investigated by using flood routing models, which do not consider the erosion and deposition processes of sediment particles in the river bed (Bajracharya et al., 2007b; Wang et al., 2008; Shrestha et al., 2010). In this context, a numerical model was developed to compute the characteristics of the outburst of glacial lake due to moraine dam failure by seepage flow and overtopping. Numerical analyses of seepage and moraine dam failure was also performed. To compute the pore water pressure in the moraine dam and slope stability of the dam, a seepage flow model and a slope stability model were incorporated into a numerical model of flow and dam surface erosion. The simulated results were compared with the experimental results.

4.1 Flow and dam surface erosion model

The flow and erosion model to predict glacial lake outburst due to moraine dam failure was developed by using the two-dimensional momentum equations of sediment-mixture flow, continuity equation of the flow and continuity equation of the sediment particles, which can be expressed as

$$\frac{\partial M}{\partial t}+\beta\frac{\partial(uM)}{\partial x}+\beta\frac{\partial(vM)}{\partial y}=gh\sin\theta_{bx0}-gh\cos\theta_{bx0}\frac{\partial(z_b+h)}{\partial x}-\frac{\tau_{bx}}{\rho_T} \quad (4)$$

$$\frac{\partial N}{\partial t}+\beta\frac{\partial(uN)}{\partial x}+\beta\frac{\partial(vN)}{\partial y}=gh\sin\theta_{by0}-gh\cos\theta_{by0}\frac{\partial(z_b+h)}{\partial y}-\frac{\tau_{by}}{\rho_T} \quad (5)$$

$$\frac{\partial h}{\partial t}+\frac{\partial M}{\partial x}+\frac{\partial N}{\partial y}=i_b\{c_*+(1-c_*)s_b\}-q \quad (6)$$

$$\frac{\partial(ch)}{\partial t}+\frac{\partial(cM)}{\partial x}+\frac{\partial(cN)}{\partial y}=i_b c_* \quad (7)$$

where $M(=uh)$ and $N(=vh)$ are the flow discharge per unit width in x and y directions, u and v are the velocity components in x and y directions, h is the flow depth, z_b is the erosion or deposition thickness measured from the original bed elevation, θ_{bx0} and θ_{by0} are the x and y components of the slope of the original bed surface, i_b is the erosion/deposition velocity, c is the sediment concentration in the flow, c_* is the maximum sediment concentration in the bed, β is the momentum correction factor equal to 1.25 for stony debris flow (Takahashi et al., 1992) and to 1.0 for both an immature debris flow and a turbulent flow, g is the acceleration due to gravity, ρ_T is the mixture density ($\rho_T=\sigma c+(1-c)\rho$, σ is density of the sediment particle and ρ is density of the water), τ_{bx} and τ_{by} are the bottom shear stresses in x and y directions, s_b is the degree of saturation in the bed and q is the infiltration rate.

The equation for the change of bed surface elevation is expressed as

$$\frac{\partial z_b}{\partial t}+i_b=0 \quad (8)$$

The bottom resistance for a two-dimensional flow is described as follows (Takahashi, 1991; Takahashi et al., 1992). For a fully developed stony debris flow ($c > 0.4c_*$);

$$\tau_{bx} = \frac{\rho_T}{8}\left(\frac{d_m}{h}\right)^2 \frac{u\sqrt{u^2+v^2}}{\{c+(1-c)\rho/\sigma\}\{(c_*/c)^{1/3}-1\}^2} \tag{9}$$

$$\tau_{by} = \frac{\rho_T}{8}\left(\frac{d_m}{h}\right)^2 \frac{v\sqrt{u^2+v^2}}{\{c+(1-c)\rho/\sigma\}\{(c_*/c)^{1/3}-1\}^2} \tag{10}$$

For an immature debris flow ($0.01 \le c \le 0.4c_*$);

$$\tau_{bx} = \frac{\rho_T}{0.49}\left(\frac{d_m}{h}\right)^2 u\sqrt{u^2+v^2} \tag{11}$$

$$\tau_{by} = \frac{\rho_T}{0.49}\left(\frac{d_m}{h}\right)^2 v\sqrt{u^2+v^2} \tag{12}$$

For a turbulent flow ($c < 0.01$);

$$\tau_{bx} = \frac{\rho g n^2 u\sqrt{u^2+v^2}}{h^{1/3}} \tag{13}$$

$$\tau_{by} = \frac{\rho g n^2 v\sqrt{u^2+v^2}}{h^{1/3}} \tag{14}$$

in which d_m is the mean particle size and n is the Manning's roughness coefficient.

The erodible bed thickness of earthen dam at each calculation time step may be partly saturated and partly unsaturated. Usually top surface close to flowing water is saturated (Nakagawa et al., 2011). In saturated region, there is no effect of suction in the soil mass. However, in unsaturated region, the suction effects in the erosion of soil. Therefore, the erosion process of moraine dam was computed by considering both the saturated and unsaturated erosion mechanism (Utsumi, 2009; Nakagawa et al., 2011). The erosion velocity equation given by Takahashi et al. (1992) for unsaturated bed without considering suction is described as

$$\frac{i_{bsat}}{\sqrt{gh}} = K_e \sin^{3/2}\theta_b \left\{1-\frac{\sigma-\rho}{\rho}c\left(\frac{\tan\phi}{\tan\theta_b}-1\right)\right\}^{1/2} \cdot \left(\frac{\tan\phi}{\tan\theta_b}-1\right)(c_\infty - c)\frac{h}{d_m} \tag{15}$$

where i_{bsat} is the erosion rate without considering suction, K_e is the erosion rate constant, c_∞ is the equilibrium sediment concentration, ϕ is the angle of internal friction, θ_b is the slope of the channel and the value of $\tan\theta_b$ in the above equations was used the energy gradient as follows:

$$\tan\theta_b = \sqrt{\tau_{bx}^2+\tau_{by}^2}\,/(\rho_T g h) \tag{16}$$

The equilibrium sediment concentration in Eq. (15) is expressed as

$$c_\infty = \frac{\rho\tan\theta_b}{(\sigma-\rho)(\tan\phi-\tan\theta_b)} \tag{17}$$

The erosion velocity equation for unsaturated bed considering suction is described as (Utsumi, 2009; Nakagawa et al., 2011)

$$\frac{i_{bunsat}}{\sqrt{gh}} = K_e \sin^{3/2}\theta_b \left\{1-\frac{\sigma-\rho}{\rho}c\left(\frac{\tan\phi}{\tan\theta_b}-1\right)-\frac{\Delta\tau_{suc}}{\rho g h\sin\theta_b}\right\}^{1/2} \left(\frac{\tan\phi}{\tan\theta_b}-1\right)(c_{\infty suc}-c)\frac{h}{d_m} \tag{18}$$

$$\Delta\tau_{suc} = \rho g|\psi|\left(\frac{\theta-\theta_r}{\theta_s-\theta_r}\right)\tan\phi \tag{19}$$

where i_{bunsat} is the erosion rate considering suction, $\Delta\tau_{suc}$ is the shear stress increment due to the suction and $c_{\infty suc}$ is the equilibrium sediment concentration considering suction, which is expressed as

$$c_{\infty suc} = \frac{\rho\tan\theta_b - \dfrac{\Delta\tau_{suc}}{gh\cos\theta_b}}{(\sigma-\rho)(\tan\phi-\tan\theta_b)} \tag{20}$$

The total erosion rate considering both with and without suction effect is expressed as

$$i_b = f\cdot i_{bsat} + (1-f)\cdot i_{bunsat} \tag{21}$$

where f is the variable based on thickness of saturated part of total eroded thickness ($0 < f < 1$) and $f = 0.5$ is used as Nakagawa et al. (2011) for the computation.

The used deposition velocity equation is expressed as follows (Takahashi et al., 1992):

$$i_b = \delta_d \frac{c_\infty - c}{c_*} \sqrt{u^2 + v^2} \tag{22}$$

where δ_d is the deposition coefficient.

4.2 Seepage flow model

A seepage flow model and a slope stability model were incorporated into a numerical model of flow and dam surface erosion. The change in pore water pressure through unsaturated-saturated soils of the moraine dam was computed by using Richards' equation as follows:

$$\frac{\partial}{\partial x}\left(K_x \frac{\partial \psi}{\partial x}\right) + \frac{\partial}{\partial z}\left(K_z\left(\frac{\partial \psi}{\partial z} + 1\right)\right) = C\frac{\partial \psi}{\partial t} \tag{23}$$

where ψ is the water pressure head, K_x and K_z are the hydraulic conductivity in x and z directions, C $\left(=\partial\theta/\partial\psi\right)$ is the specific moisture capacity, θ is the volumetric water content of soil, x is the horizontal spatial coordinate, z is the vertical spatial coordinate taken as positive upwards and t is the time. The relationships of water storage coefficient and the coefficient of permeability are very important to compute the moisture movement in the unsaturated-saturated soil system using Eq. (23). Thus, the seepage flow analyses in the moraine dam were performed using the widely used constitutive relationships given by van Genuchten (1980) and Brooks and Corey (1964). The constitutive relationships given by van Genuchten (1980) were used to compute the water storage coefficient, the coefficient of permeability and the specific moisture capacity as

$$S_e = \frac{\theta - \theta_r}{\theta_s - \theta_r} = \begin{cases} \dfrac{1}{\left(1 + |\alpha\psi|^\eta\right)^m} & if\ \psi < 0 \\ 1 & if\ \psi \geq 0 \end{cases} \tag{24}$$

$$K = \begin{cases} K_s S_e^{0.5}\left[1 - (1 - S_e^{1/m})^m\right]^2 & if\ \psi < 0 \\ K_s & if\ \psi \geq 0 \end{cases} \tag{25}$$

$$C = \begin{cases} m\left\{1 + (|\alpha\psi|)^\eta\right\}^{-m-1}\eta(|\alpha\psi|)^{\eta-1}\alpha(\theta_s - \theta_r) & if\ \psi < 0 \\ 0 & if\ \psi \geq 0 \end{cases} \tag{26}$$

where S_e is the effective saturation, θ_s and θ_r are the saturated and residual moisture content of the sediment mix respectively, α and η are the parameters related with matric potential of soil and are determined by using a curve fitting of soil-water retention curve, K_s is the saturated hydraulic conductivity and $m = 1 - 1/\eta$.

The water storage coefficient, the coefficient of permeability and the specific moisture capacity given by Brooks and Corey (1964) are described as

$$S_e = \frac{\theta - \theta_r}{\theta_s - \theta_r} = \begin{cases} (|\psi/\psi_b|)^{-\lambda} & if\ \psi < \psi_b \\ 1 & if\ \psi \geq \psi_b \end{cases} \tag{27}$$

$$K = \begin{cases} K_s S_e^{\ \delta} & if\ \psi < \psi_b \\ K_s & if\ \psi \geq \psi_b \end{cases} \tag{28}$$

$$C = \begin{cases} \lambda(|1/\psi_b|)^{-\lambda}|\psi|^{(-\lambda-1)}(\theta_s - \theta_r) & if \psi < \psi_b \\ 0 & if \psi \geq \psi_b \end{cases} \tag{29}$$

where ψ_b is the air-entry value, λ is the pore-size distribution index and $\delta\left(=(2+3\lambda)/\lambda\right)$ is an empirical constant.

4.3 Slope stability model

Numerous slope stability analysis approaches are available. Many researchers used the simplified Janbu's method to calculate the factor of safety F_s for slip surface as (Takahashi, 1991)

$$F_s = \frac{1}{\sum_{i=1}^{n} W_i \tan\alpha_i} \cdot \sum_{i=1}^{n} \frac{c' l_i \cos\alpha_i + \left(W_i - u_{wi} l_i \cos\alpha_i\right)\tan\phi}{\cos^2\alpha_i\left(1 + \tan\alpha_i \tan\phi / F_s\right)} \tag{30}$$

in which c' is the cohesion of the material of the dam body, l_i is the length of the base of each slice, α_i is the slope of the bottom of each slice, W_i is the weight of each slice including surface water, u_{wi} is the average pore water pressure on the bottom of each slice and ϕ is the angle of internal friction.

The simplified Janbu's method does not consider the negative pore water pressures developed in the unsaturated soils. The negative pore water pressure causes the shear strength to

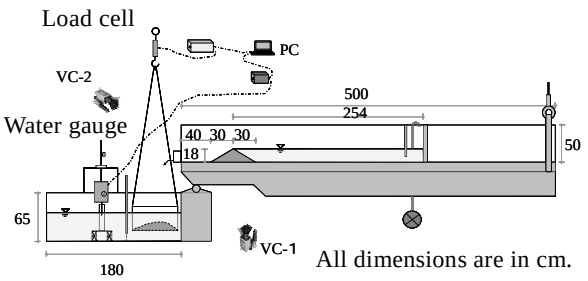

Fig. 27 Experimental flume setup

increase. Thus, the shear strength (τ) for an unsaturated soil is defined as (Vanapalli et al., 1996)

$$\tau = c' + (\sigma_n - u_a)\tan\phi + (u_a - u_w)\left(\frac{\theta - \theta_r}{\theta_s - \theta_r}\right)\tan\phi \quad (31)$$

in which σ_n is the total normal stress, u_a is pore-air pressure and u_w pore-water pressure. By using the shear strength equation Eq. (31), the factor of safety for slip surface can be defined as

$$F_s = \frac{\sum_{i=1}^{n} c' l_i + (P_i - u_{ai} l_i)\tan\phi + (u_{ai} - u_{wi}) l_i \left(\frac{\theta - \theta_r}{\theta_s - \theta_r}\right)_i \tan\phi}{W_i \sin\alpha_i} \quad (32)$$

$$P_i = \left[W_i - \frac{1}{F_s}\left\{ \left(c' + (u_{ai} - u_{wi})(\theta - \theta_r)_i / (\theta_s - \theta_r)\tan\phi\right) l_i \sin\alpha_i - u_{ai} l_i \tan\phi \sin\alpha_i \right\} \right] / m_{\alpha i} \quad (33)$$

$$m_{\alpha i} = \cos\alpha_i (1 + \tan\alpha_i \tan\phi / F_s) \quad (34)$$

4.4 Flume experiments and methods

A series of experiments were carried out to investigate the failure mechanism of moraine dam and developed numerical model was verified with the experimental results. A 500cm long, 30cm wide and 50cm deep flume was used for the experiments (Fig. 27). A dam body was made by silica sand (Sediment mix 1-6 and Sediment mix 1-7). Two types of sediment mixes were used for the comparison of the results with different grain size. Figs. 28 and 29 show the grain size distribution curve and the details of the dams, respectively. The mean diameter (d_m) of sediment mixes 1-6 and 1-7 are 1.4mm and 1.04mm, respectively. The maximum particle size ($d_{\max}$) and sediment density (σ) of both sediment mixes 1-6 and 1-7 are

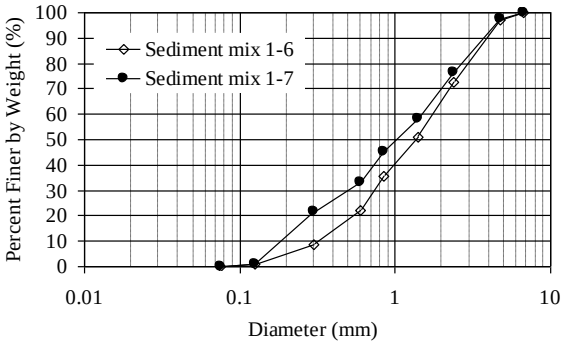

Fig. 28 Particle size distribution of bed sediment

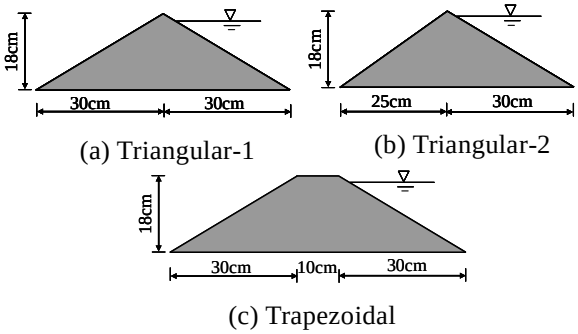

Fig. 29 Details of different types of dam body

Table 1 Experimental conditions

Case	Supply discharge Q (cm^3/sec)	Discharge supply time (sec)	Sediment mixture	Dam shape
Case-I	975	200	Mix 1-6	Trapezoidal
Case-II	975	200	Mix 1-6	Trianguler-1
Case-III	975	200	Mix 1-6	Trianguler-1
Case-IV	927	128	Mix 1-6	Trianguler-2
Case-V	895	130	Mix 1-7	Trianguler-2

4.75mm and 2.65g/cm^3, respectively.

The lake water was filled by supplying a constant water discharge from the upstream end of the lake. In the case of moraine dam failure by overtopping due to water level rising, the constant water discharge was supplied continuously from upstream end of the lake to overtop the dam and erode it. However, in the case of moraine dam failure by seepage, the lake water was filled up to about 16cm in depth by supplying constant water discharge from the upstream end of the lake. The details of the experimental conditions are shown in Table 1. The outflow discharge and sediment discharge were measured by using servo type water gauge and load cell, respectively. The temporal variations of the shapes of dam body due to erosion were captured by two video cameras located at the

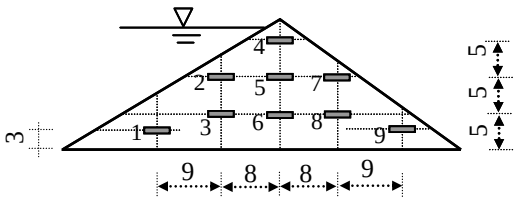

All dimensions are in cm.

Fig. 30 Position of 1 to 9 WCRs in the dam body

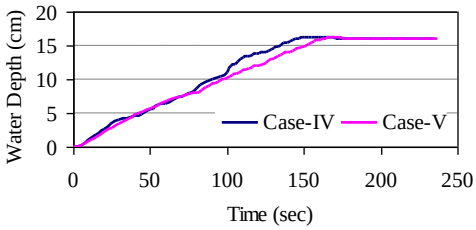

Fig. 31 Measured temporal variation of lake water depth

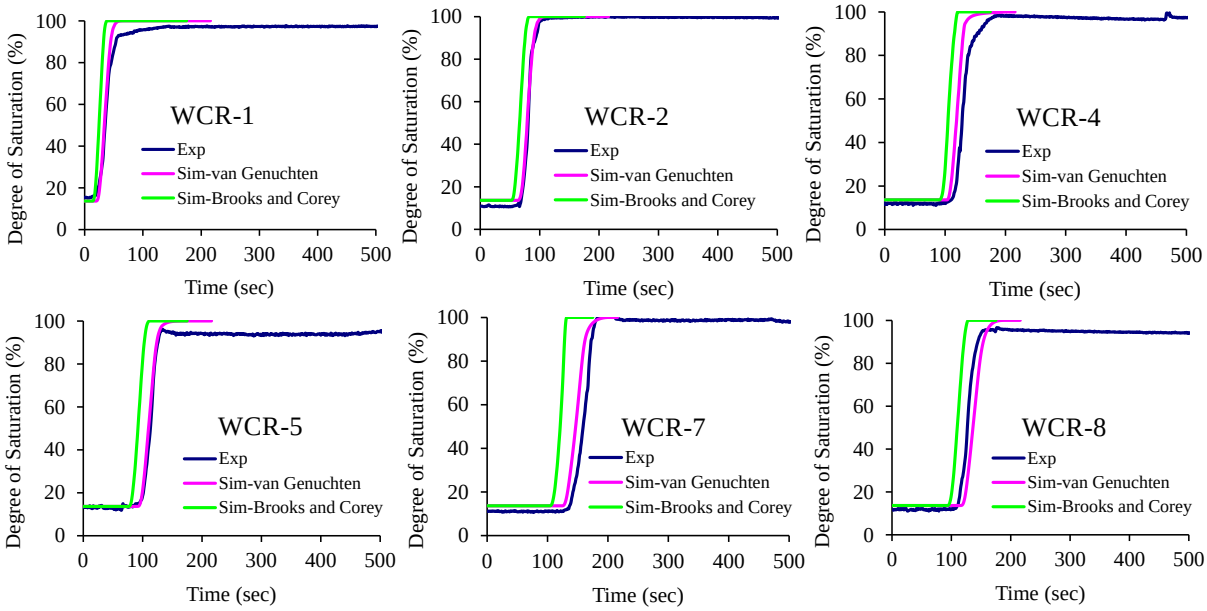

Fig. 32 The simulated and experimental moisture content profile, Case-IV (sediment mix 1-6 case)

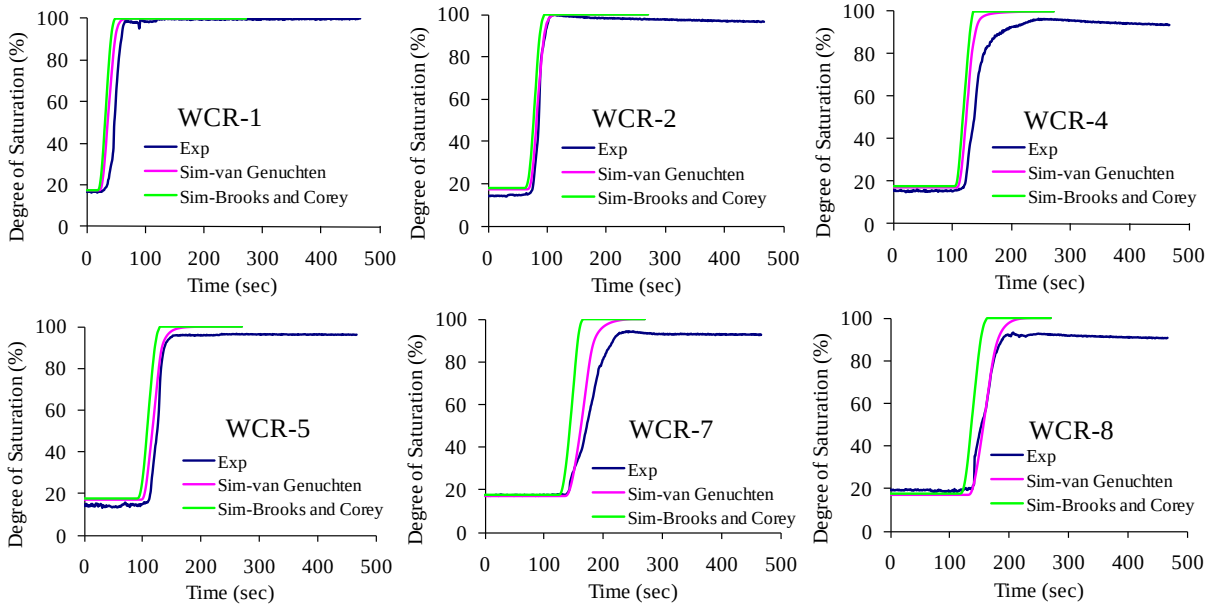

Fig. 33 The simulated and experimental moisture content profile, Case-V (sediment mix 1-7 case)

side and the top of the flume. The moisture movement in the dam body was measured by using the Water Content Reflectometers (WCRs) at different nine locations (Fig. 30).

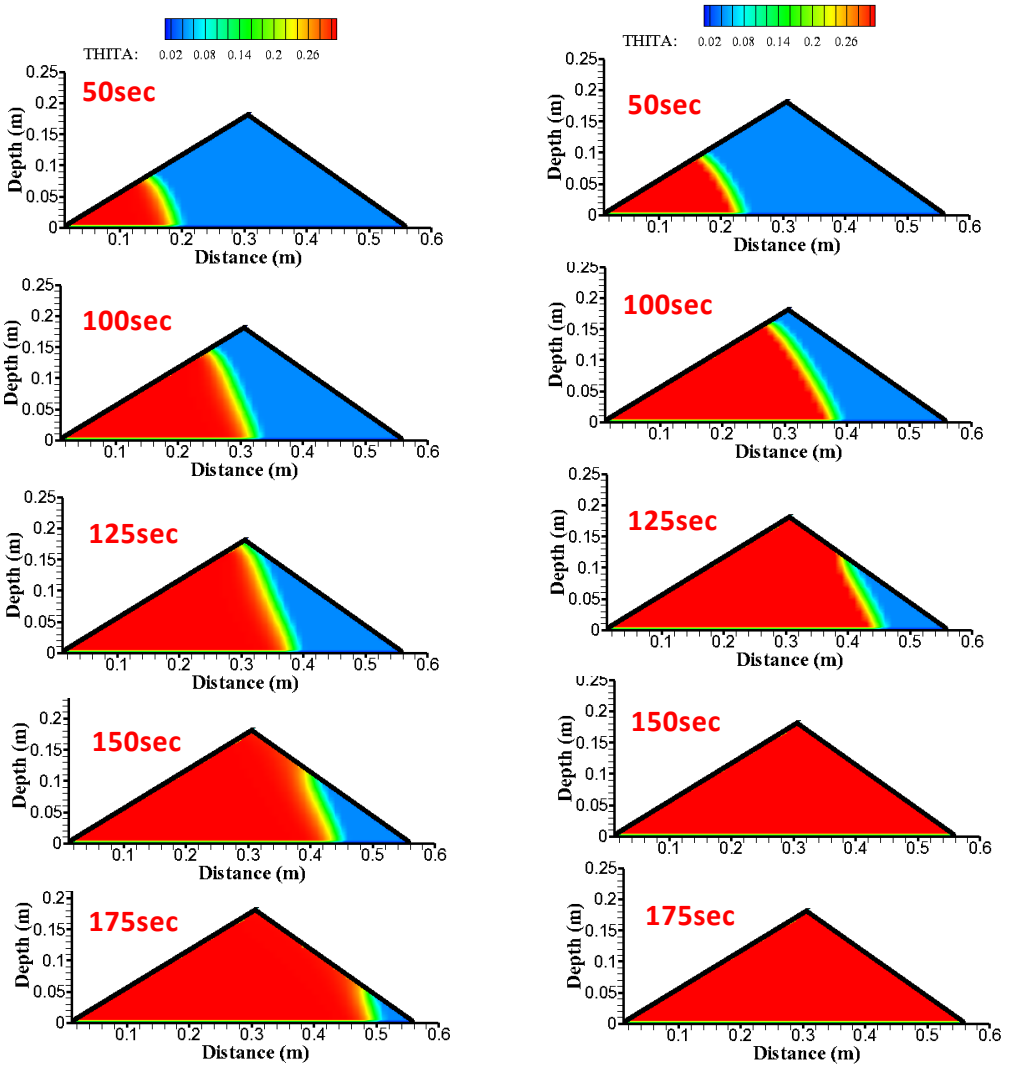

(a) Using van Genuchten (1980) (b) Using Brooks and Corey (1964)

Fig. 34 Comparison of moisture movement in the dam body by using van Genuchten (1980) and Brooks and Corey (1964) constitutive relationships, Case IV

4.5 Results and discussions of numerical analysis

By using developed model, seepage analysis in the dam body, slope stability of the dam and failure of moraine dam due to seepage and overtopping were analyzed for the flume experimental cases. Fig. 31 shows the measured temporal water depth in the lake. The values of the soil parameters of the constitutive relationships of van Genuchten (α=6.3, $\eta=3.1$ and α=4.0, $\eta=$ 3.2 for sediment mixes 1-6 and 1-7) and Brooks and Corey (λ=2.5, ψ_b=-0.19 and λ=1.8, ψ_b=-0.19 for sediment mixes 1-6 and 1-7) were determined by using a curve fitting of soil-water retention curve of the both sediment mixes (see Appendix). The measured values $K_s=0.0005m/\sec$ and $\theta_s=0.312$ for sediment mix 1-6 and $K_s=0.00025m/\sec$ and $\theta_s=0.296$ for sediment mix 1-7 were used. Fig. 32 and Fig. 33 show the simulated and experimental moisture profile in the dam body in Case-IV and Case-V, respectively. The time, *t*=0sec, in the figures is the starting time of water supply from the upstream end of the lake. Fig. 34 shows the comparison of temporal variation of moisture movement in the dam body by using van Genuchten (1980) and Brooks and Corey (1964) constitutive relationships in Case-IV. The moisture movement in the dam body is due to the depth of the lake water in the upstream. The moisture movement in the dam by using Brooks and Corey relationships is faster than the experimental. The hydraulic conductivity in the unsaturated soil is higher in the Brooks and Corey relations than van Genuchten.

The simulated results by using the constitutive relations of van Genuchten are more agreeable with the experimental results than the Brooks and Corey relationships. The relationships of water storage coefficient and the coefficient of permeability are very important to compute the moisture movement in the unsaturated region. The moisture movement in the dam also depends on the saturated hydraulic conductivity. The sediment mix 1-7 contains higher fine sediments than in sediment mix 1-6 and the moisture movement is slower in sediment mix 1-7 than in case of sediment mix 1-6 due to the smaller hydraulic conductivity in this case.

Fig. 35 shows the comparison of the simulated slip surfaces of moraine dam failure due to seepage with considering suction and without considering suction (Janbu's simplified method) in the shear strength of the soil with the experimental slip surfaces. The moisture movement in the soil was calculated by using van Genuchten relationships. The dynamic programming method was used to compute the critical slip surfaces (Shrestha et al., 2010a). The simulated failure surfaces considering the suction in slope stability analysis are more agreeable with the experimental results than the Janbu's simplified method. In unsaturated soils, the failures are generally characterized by shallow failure surfaces. Without considering the effect of the matric suction in the slope stability analysis, deep failure surface may occur. Thus, the unsaturated shear strength with the matric suction is necessary to consider in the slope stability analysis of the unsaturated dam body. The failure surface is deeper in the case of sediment mix 1-6 than sediment mix 1-7, which may be due to the higher effect of suction in sediment mix 1-7.

To calculate the outburst discharge of moraine dam failure, hereafter van Genuchten relationships were used in the seepage calculation and the slope stability analysis was carried out by considering the suction in the unsaturated soil. Fig. 36 shows the simulated and experimental results of the outburst discharge and accumulated discharge at the downstream end of the flume due to moraine dam failure by water overtopping (Case-I). In this case, the initial moisture content in the dam is about 0.21%. In the figures, the time t=0sec is the starting time of discharge outflow at the downstream end of the flume. Fig. 37 shows the temporal variation of the dam surface erosion by water overtopping. The

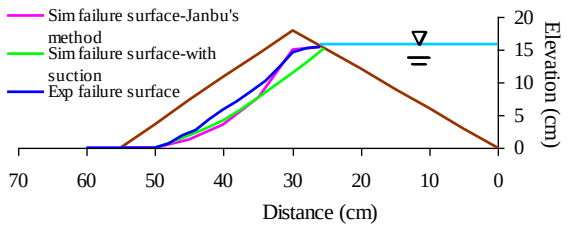

(a) Sediment mix 1-6 (Case-IV)

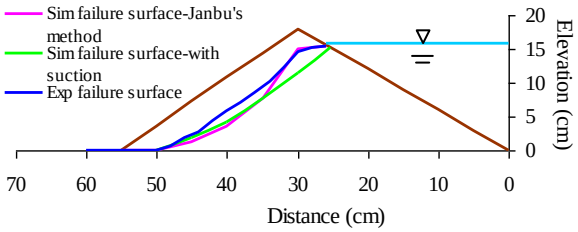

(b) Sediment mix 1-7 (Case-V)

Fig. 35 Simulated and experimental slip surface

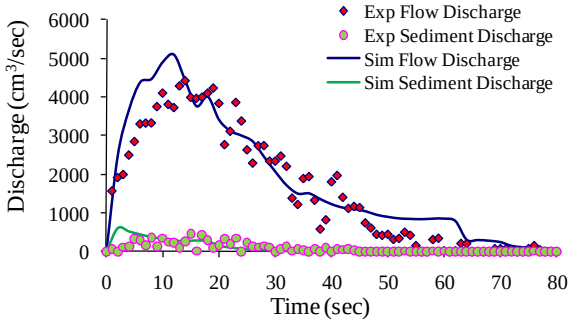

(a) Outflow discharge

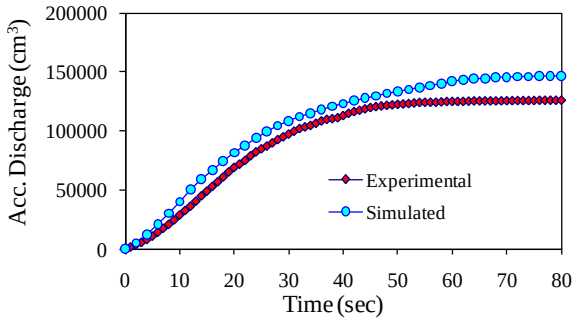

(b) Accumulated flow discharge

Fig. 36 Simulated and experimental results of outflow discharge and accumulated discharge, Trapezoidal dam case (CASE-I)

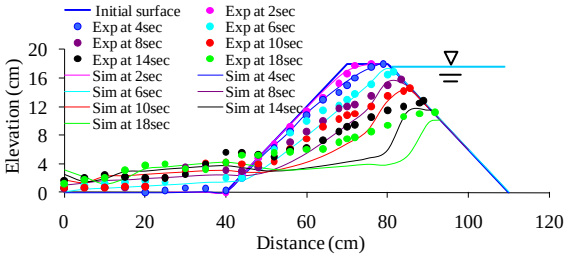

Fig. 37 Temporal variations of dam surface due to erosion, Case-I, time t=0sec is the starting time of erosion, 0.21% initial moisture content

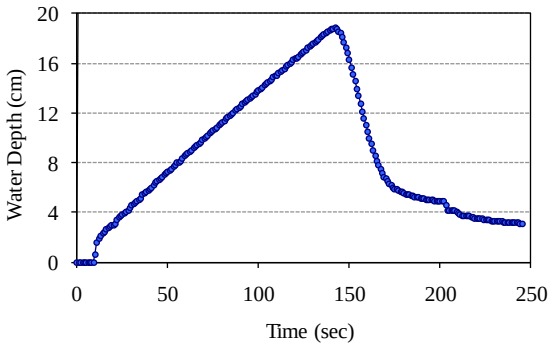

Fig. 38 Temporal variations of water depth at just upstream of upstream end of moraine dam, Case-I

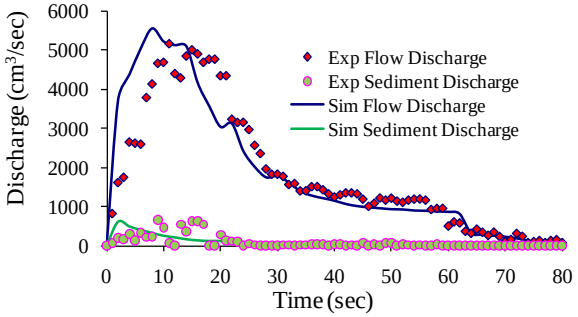

(a) Outflow discharge

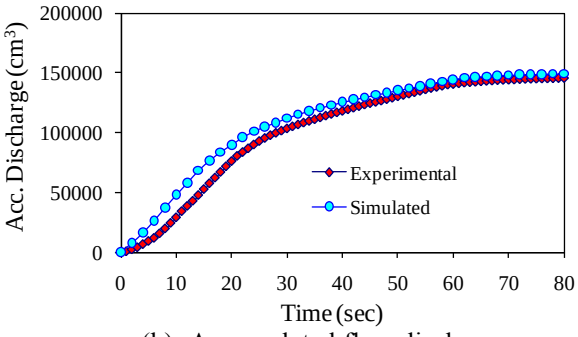

(b) Accumulated flow discharge

Fig. 39 Simulated and experimental results of outflow discharge and accumulated discharge, Triangular dam case (CASE-II)

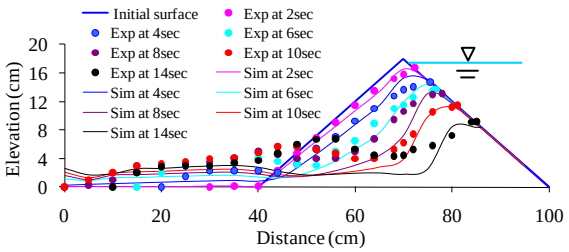

Fig. 40 Temporal variations of dam surface due to erosion, Case-II, time *t*=0sec is the starting time of erosion, 0.21% initial moisture content

simulated results were agreeable with the experimental results. The temporal variation of water filling up and drawdown at just upstream of

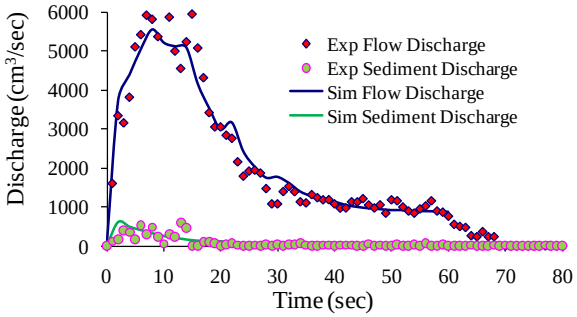

(a) Outflow discharge

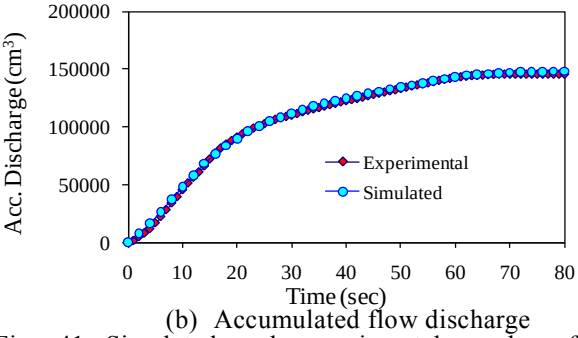

(b) Accumulated flow discharge

Fig. 41 Simulated and experimental results of outflow discharge and accumulated discharge, Triangular dam case (CASE-III)

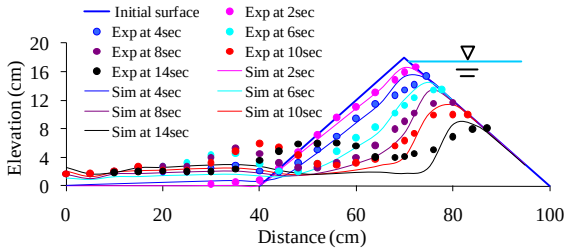

Fig. 42 Temporal variations of dam surface due to erosion, Case-III, time t=0sec is the starting time of erosion, 5.54% initial moisture content

the upstream end of dam in the lake is shown in Fig. 38. Fig. 39 shows the outburst discharge and accumulated discharge at the downstream end of the flume in the case of triangular dam (Case-II). The initial moisture content in the dam is about 0.21%. Fig. 40 shows the temporal variation of dam surface in the case of triangular dam (Case-II). Fig. 41 shows the results of the outburst discharge due to moraine dam failure by overtopping with 5.54% initial moisture content in the dam (Case-III). The peak discharge is higher in the case of 5.54% initial moisture content in the dam. Fig. 42 shows the dam surface erosion by water overtopping in Case-III. It was found that the peak discharge was higher in the case of triangular shape dam than trapezoidal shape. The simulated results of the outburst discharge in

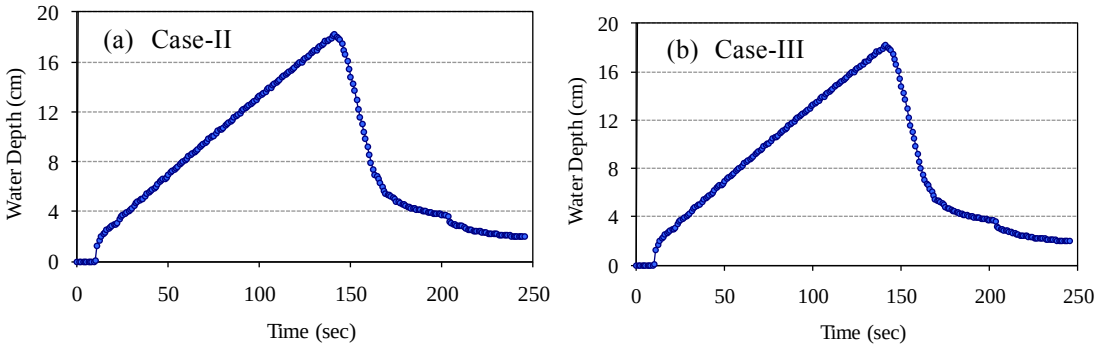

Fig. 43 Temporal variations of water depth at just upstream of the upstream end of moraine dam, Case-II and Case-III

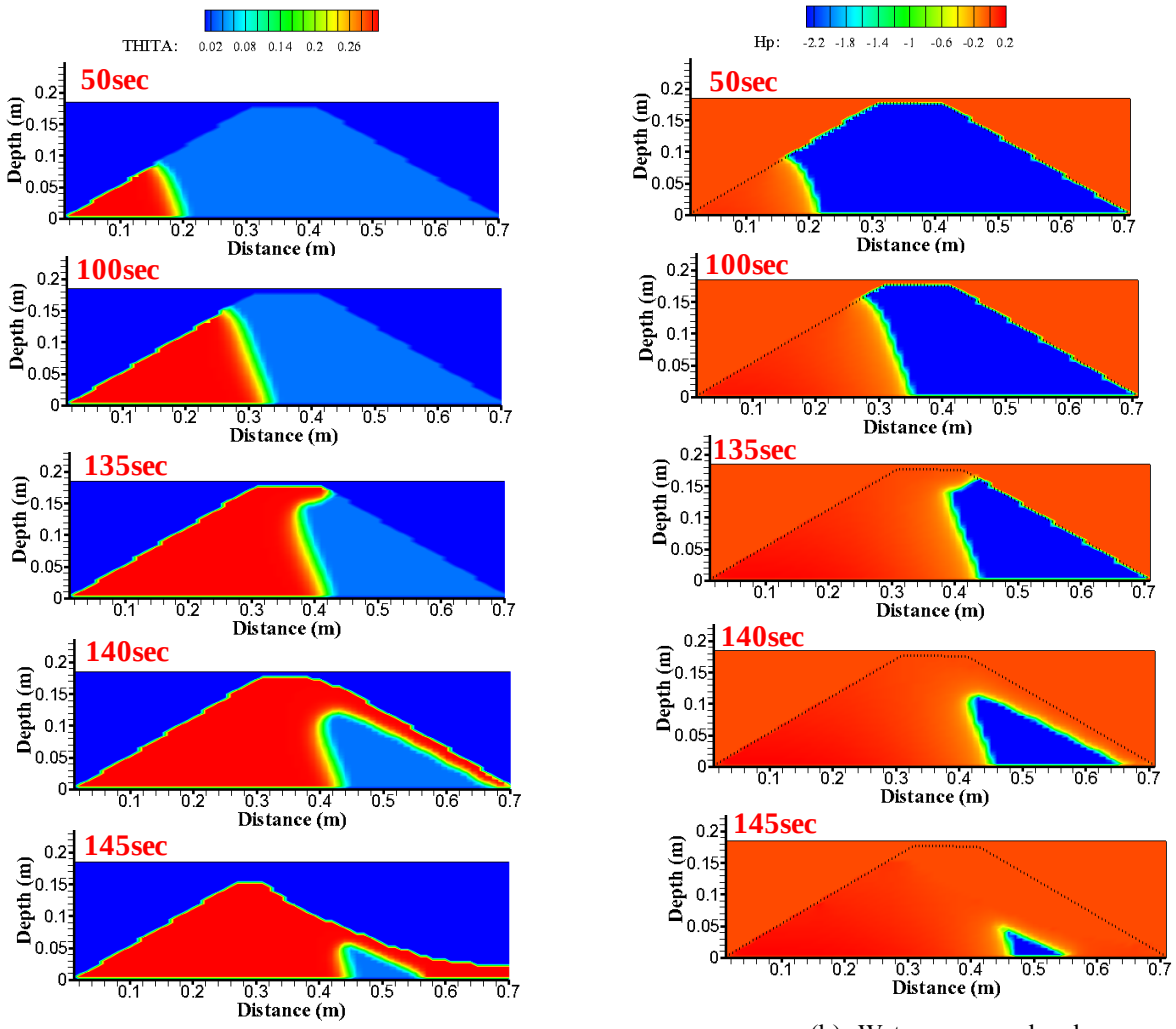

(a) Moisture content (b) Water pressure head

Fig. 44 Temporal variation of moisture content and pressure head in the dam, Case-I

the all three cases agreed with the experimental results. The effect of suction in the soil was also considered in the dam surface erosion. The erosion of moraine dam by overtopping was also well explained by the numerical simulation model. Fig. 43 shows the simulated results of temporal variation of lake water filling up and water drawdown due to moraine dam failure at just upstream of the upstream end of the dam in Case-II and Case-III.

Fig. 44 shows the simulated results of temporal variation of moisture content and pressure head in the trapezoidal dam (Case-I). Similar results of the

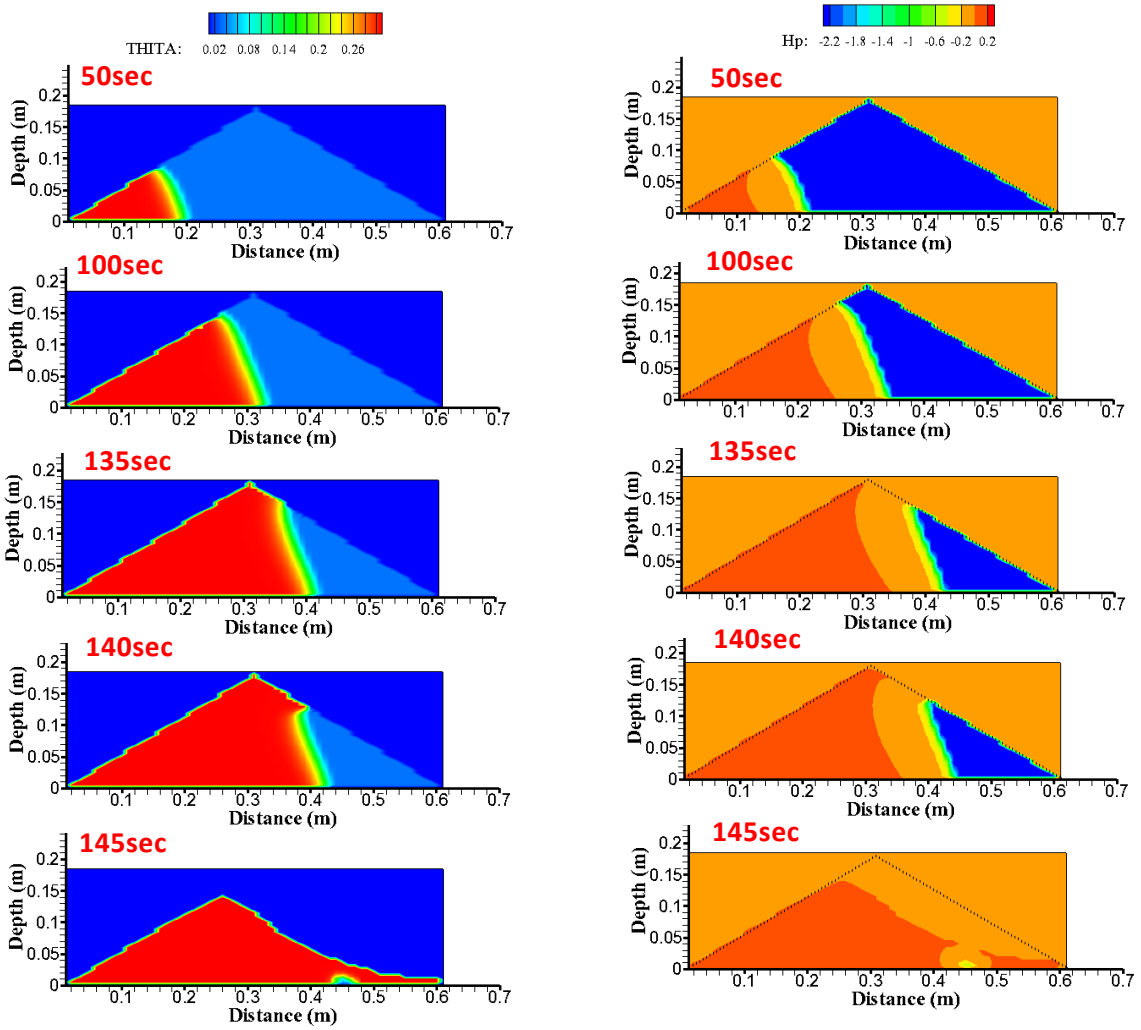

(a) Moisture content (b) Water pressure head

Fig. 45 Temporal variation of moisture content and pressure head in the dam, Case-II

temporal variation of moisture content and pressure head in Case-II and Case-III are shown in Figs. 45 and 46, respectively. The temporal variation of moisture content and pressure head in both trapezoidal and triangular dam cases were well explained by numerical simulations. The equations of seepage flow model were solved by Line Successive Over Relaxation (LSOR) scheme with an implicit iterative finite difference schemes as used by Freeze (1971, 1978). The partial differential equations of basic equations of flow and erosion model were obtained from the methods adopted by Nakagawa (1989) by using Leap-Frog scheme, in which upwind scheme was adopted in the advection term and implicit scheme was introduced in the friction term.

Fig. 47 shows the simulated and experimental results of the outburst discharge in the case of moraine dam failure by seepage for sediment mixes 1-6 and 1-7. Immediately after failure of moraine dam, the lake water overtopped the dam and eroded it, which results the rapid drawdown of lake water. The peak discharge in the case of sediment mix 1-6 is higher than in the case of sediment mix 1-7. In the case of moraine dam failure by seepage also, the simulated results of outburst discharge at the flume end were agreeable with the experimental results. The accumulated discharges in the case of moraine dam failure by seepage cases are shown in Fig. 48. The comparisons of the simulated and experimental results show that the two-dimensional flow and erosion model used in this study gives stable and reliable results. The proposed model can be used to compute the characteristics of glacial lake outburst

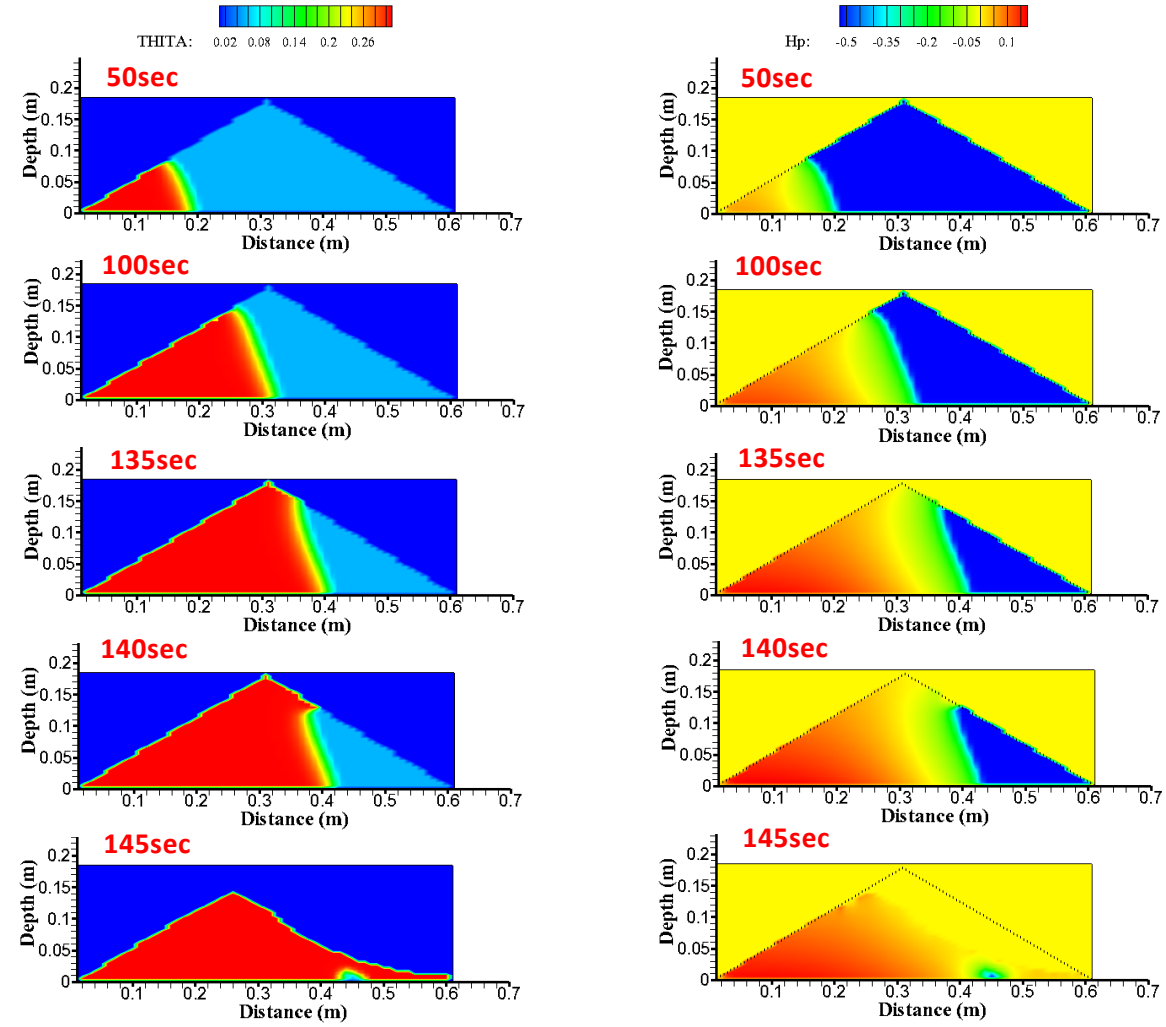

(a) Moisture content (b) Water pressure head

Fig. 46 Temporal variation of moisture content and pressure head in the dam, Case-III

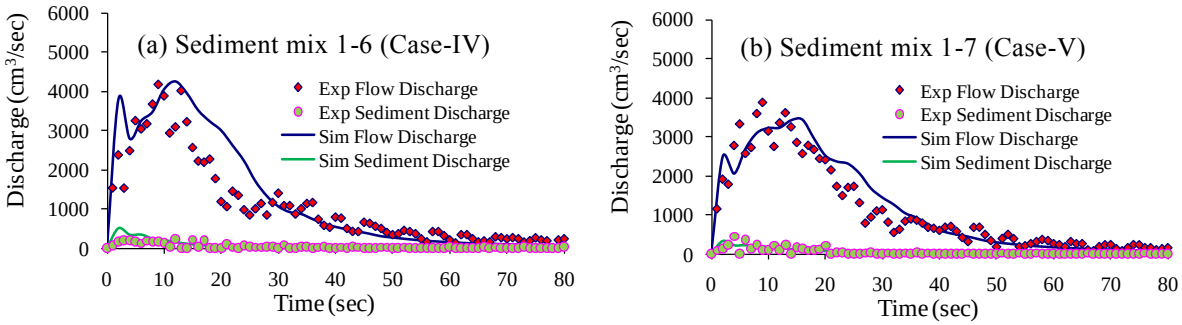

Fig. 47 Outflow hydrograph in case of moraine dam failure by seepage (Case-IV and Case-V)

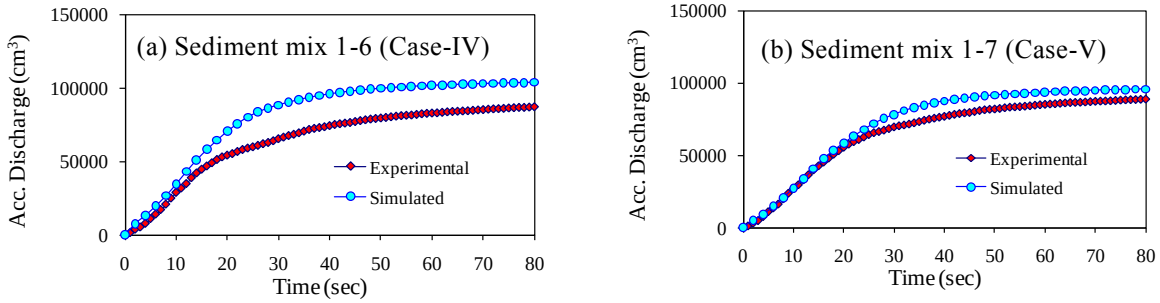

Fig. 48 Accumulated discharge in case of moraine dam failure by seepage (Case-IV and Case-V)

due to moraine dam failure by seepage flow and lake water overtopping.

By using this developed numerical model, we are analyzing potential outburst flood from Tsho Rolpa Glacial Lake in the Rolwaling valley of Nepal. This lake is most dangerous and largest lake in Nepal. The outburst from this lake may cause serious damages and loss of lives. Thus, it is very urgent to analyze the catastrophic glacial outburst flood from Tsho Rolpa Glacial Lake and to investigate their downstream impact to society.

5. Conclusions

The assessment of glacial hazards in the Rolwaling valley of Nepal had been presented. Based on the field visit at Tsho Rolpa Glacial Lake, it was observed that the moraine dam of this lake can be breached due to sudden collapse of dam by seepage and due to erosion by wave overtopping by falling of steeply hanging glaciers in the right side of the lake. The area of glacial lakes in the Himalaya is rapidly increasing in trend due to impact of global climate change, which may cause outburst of glacial lake. Hazards/disasters due to GLOF are likely to increase in intensity with the impacts of climate change.

The numerical analyses were carried out to compute the characteristics of glacial lake outburst due to moraine dam failure by seepage and overtopping. The moisture profile calculated by using van Genuchten was more agreeable with the experimental moisture profile. The simulated failure surface considering the suction in slope stability analysis gave more accurate results than Janbu's simplified method. The results of the outburst discharge and dam surface erosion also agreed with the experimental results. The sudden release of outburst discharge from the lake may cause the catastrophic disasters and flooding in downstream.

In our further study, the characteristics of flood disasters and hazardous zone caused by outburst of most potential dangerous glacial lake Tsho Rolpa of Nepal has been preparing by using developed numerical model and Geographical Information System (GIS) tools with various scenarios.

Acknowledgements

The authors are grateful to the GCOE program 'Sustainability/Survivability Science for a Resilient Society Adaptable to Extreme Weather Conditions' of Disaster Prevention Research Institute, Kyoto University for providing financial support for this research work and also for providing Young Scientist Research Grant to the first author. The authors are also wish to thank Mr. Shiro Nakanishi (Master course student, Graduate School of Engineering, Kyoto University) for his help in translation of English synopsis into Japanese. The authors are also grateful to Prof. Narendra Man Shakya and Dr. Raghu Nath Jha, Institute of Engineering, Pulchowk Campus, Nepal for their suggestions and help during field visit. The authors are also thanks to Mr. Pradeep Kumar Mool, Remote Sensing Specialist, ICIMOD, Nepal for providing information about Tsho Rolpa Glacial Lake.

References

Bajracharya, O. R. (2008): Himalayan glacier and Glacier Lake Outburst Flood (GLOF), SAARC Workshop on Climate Change and Disaster: Emerging Trends and Future Strategies, Kathmandu Nepal, http://www.nset.org.np/nset/climatechange/presentation/d1_s2/np/Om%20R%20Bajracharya_Glacier_GLOF%20v2.0.pdf (online accessed on 2011-05-06).

Bajracharya, S. R. (2010): Glacial lake outburst flood disaster risk reduction activities in Nepal, International Journal of Erosion Control Engineering, JSECE, Vol. 3, No. 1, pp.92-101.

Bajracharya, S. R., Mool, P. K., and Shrestha, B. R. (2006): The impact of global warming on the glaciers of the Himalaya, International Symposium on Geo-disasters, Infrastructure Management and Protection of World Heritage Sites, Nepal Engineering College, Ehime University and National Society for Earthquake Technology Nepal, pp.231-242.

Bajracharya, S. R., Mool, P. K., and Shrestha, B. R. (2007a): Impact of climate change on Himalayan glaciers and glacial lakes, case studies on GLOF and associated hazards in Nepal and Bhutan,

International Center for Integrated Mountain Development (ICIMOD) and United Nations Environment Programme (UNEP), pp.1-119.

Bajracharya, B., Shrestha, A. B. and Rajbhandari, L. (2007b): Glacial lake outburst floods in the Sagarmatha region, Mountain Research and Development, Vol. 27, No. 4, pp.336-344.

Brooks, R. H. and Corey, A. T. (1964): Hydraulic properties of porous medium, Hydrology Paper, Colorado State University (Fort Collins), Nr.3, Vol. 27.

Cenderelli, A. D. and Wohl, E. E. (2001): Peak discharge estimates of glacial-lake outburst floods and "normal" climatic floods in the Mount Everest region, Nepal, Geomorphology, Vol. 40, pp.57-90.

Clague, J. J and Evans, S. G. (2000): A review of catastrophic drainage of moraine-dammed lakes in British Columbia, Quaternary Science Reviews, Vol. 19, pp.1763-1783.

Costa, J. E. and Schuster, R. L. (1988): The formation and failure of natural dams, Geological Society of America Bulletin, Vol. 100, pp.1054-1068.

Department of Hydrology and Metrology (DHM) (2008): Streamflow Summary (1962-2006), Hydrology Division, DHM, Government of Nepal.

Dwivedi, S. K. (2005): Downstream impacts of glacier lake outburst flood in the Himalaya, Proceedings of International Conference on Monitoring, Prediction and Mitigation of Water-Related Disasters (MPMD-2005), Disaster Prevention Research Institute, Kyoto University, pp.387-393.

Evans, S. G. (1986): The maximum discharge of outburst floods caused by the breaching of man-made and natural dams, Canadian Geotechnical Journal, Vol. 23, pp.385-387.

Fread, D. L. (1988): DAMBRK: the NWS DAMBRK model: Theoretical background/user documentation, Hydrologic Research Laboratory, Office of Hydrology, NWS, NOAA.

Fread, D. L. (1991): BREACH: an erosion model for earthen dam failures, U.S. National Weather Service, Office of Hydrology, Silver Spring, Maryland.

Freeze, R. A. (1971): Influence of the unsaturated flow domain on seepage through earth dams, Water Resources Research, Vol. 7, pp.929-941.

Freeze, R. A. (1978): Mathematical models of hillslope hydrology, In M. J. Kirkby, (ed), Hillslope Hydrology, John Wiley, pp.177-225.

Horstmann, B. (2004): Glacial lake outburst floods in Nepal and Switzerland - new threats due to climate change, Germanwatch, pp.1-11. http://www.germanwatch.org/download/klak/fb-gl-e.pdf (accessed 26 April 2010).

Huggel, C., Haeberli, W., Kääb, A., Bieri, D. and Richardson, S. (2004): An assessment procedure for glacial hazards in the Swiss Alps, Canadian Geotechnical Journal, Vol. 41, pp.1068-1083.

Huggel, C., Kääb, A., Haeberli, W., Teysseire, P. and Paul, F. (2002): Remote sensing based assessment of hazards from glacier lake outbursts: a case study in the Swiss Alps, Canadian Geotechnical Journal, Vol. 39, pp.316-330.

Matambo, S. T. and Shrestha, A. B. (2011): Nepal: Responding Proactively to Glacial Hazards, World Resources Report, Washington DC, pp.1-18 (http://www.worldresourcesreport.org) (accessed 15 May 2011).

Mool, P. K. (2010): Glacial lakes and glacial lake outburst floods in the Himalayas, International Center for Integrated Mountain Development (ICIMOD), http://geoportal.icimod.org/symposium2010/PPT/Theme-I/PK%20Mool.pdf (online accessed on 2011-04-25).

Mool, P. K., Bajracharya, S. R. and Joshi, S. P. (2001): Risk assessment of Tsho Rolpa Glacial Lake along the Rolwaling and Tama Koshi valleys, Dolakha District, Nepal, United Nations Environment Programme – Asia and the Pacific (UNEP-AP) and International Center for Integrated Mountain Development (ICIMOD), http://www.rrcap.unep.org/glofnepal/Nepal/Field%20Report%20TSHO_ROLPA%20Oct.%20Y2K/complete%20Tsho%20Rolpa%20field%20report.pdf (accessed 13 May 2011).

Nakagawa, H. (1989): Study on risk evaluation of flood and sediment inundation disaster, Doctoral Thesis, Kyoto University (in Japanese).

Nakagawa, H., Utsumi, T., Kawaike, K. Baba, Y. and Zhang, H. (2011): Erosion of unsaturated river embankment due to overtopping water, Annual Journal of Hydraulic Engineering, JSCE, Keynote Lecture, Vol. 55, pp.K-1-K-4.

Osti, R. and Egashira, S. (2009): Hydrodynamic

characteristics of the Tam Pokhari glacial lake outburst flood in the Mt. Everest region, Nepal, Hydrological Processes, Vol. 23, pp.2943–2955.

Reynolds, J. M. (1999): Glacial hazard assessment at Tsho Rolpa, Rolwaling, Central Nepal, Quarterly Journal of Engineering Geology, the Geological Society of London, Vol. 32, pp.209-214.

Richardson, S. D. and Reynolds J. M. (2000): An overview of glacial hazards in the Himalayas, Quaternary International, Vol. 65-66, pp.31-47.

Shrestha, A. B., Eriksson, M., Mool, P., Ghimire, P., Mishra, B. and Khanal, N. R. (2010): Glacial lake outburst flood risk assessment of Sun Koshi basin, Nepal, Geomatics, Natural Hazards and Risk, Vol. 1 No. 2, pp.157-169.

Shrestha, B. B., Nakagawa, H., Kawaike, K., Baba, Y. and Zhang, H. (2010a): Glacial lake outburst due to moraine dam failure by seepage and overtopping with impact of climate change, the Annuals of the Disaster Prevention Research Institute, Kyoto University, No. 53, pp.569-582.

Shrestha, B. B., Nakagawa, H., Kawaike, K., Baba, Y. and Zhang, H. (2010b): Impact of global climate change on glacial lakes and glacial lake outburst floods, International Symposium on Sediment Disasters and River Environment in Mountainous Area, JSPS Asia-Africa Science Platform Program, Kyoto University, Japan, pp.53-54.

Shrestha, B. B., Nakagawa, H., Kawaike, K., Baba, Y. and Zhang, H. (2010c): Study on moraine dam failure and glacial lake outburst flood with impact of global climate change, Proceedings of International Symposium on a Robust and Resilient Society against Natural Hazards & Environmental Disasters and the third AUN/Seed-Net Regional Conference on Geo-Disaster Mitigation, Kyoto University, Japan, pp.27-37.

Shrestha, B. B., Nakagawa, H., Kawaike, K., Baba, Y. and Zhang, H. (2010d): Outburst of glacial lakes due to moraine dam failure under global climate change, Proceedings of the 29th Annual Meeting of the Japan Society for Natural Disaster Science, pp.171-172.

Takahashi, T. (1991): Debris flow, IAHR Monograph Series, Rotterdam: Balkema.

Takahashi, T., Nakagawa, H., Harada, T. and Yamashiki, Y. (1992): Routing debris flows with particle segregation, Journal of Hydraulic Engineering, ASCE, Vol. 118, No. 11, pp.1490-1507.

Utsumi, T. (2009): Study on unsaturated embankment dam failure due to overtopping, Master Thesis, Kyoto University, 2009.

U.S. Corps of Engineers (2002): HEC-RAS river analysis system hydraulic reference manual, Hydraulic Engineering Center Report, CPD-69, US Corps of Engineers: Davis.

van Genuchten, M. T. (1980): A closed-form equation for predicting the hydraulic conductivity of unsaturated soils, Soil Science Society of American Journal, Vol. 44, pp.892-898.

Vanapalli, S. K., Fredlund, D. G., Pufahl, D. E. and Clifton, A. W. (1996): Model for the prediction of shear strength with respect to soil suction, Canadian Geotechnical Journal, Vol. 33, pp.379-392.

Wang, X., Lui, S., Guo, W. and Xu, J. (2008): Assessment and simulation of glacier lake outburst floods for Longbasaba and Pida lakes, China, Mountain Research and Development, Vol. 28, No. 3/4, pp.310-317.

Water and Energy Commission Secretariat (WECS) (1993): Interim report on the field investigation on the Tsho Rolpa Glacier Lake, Rolwaling valley, WECS, Nepal Government.

Yamada, T. (1998): Glacier lake and its outburst flood in the Nepal Himalaya, Data Center for Glacier Research, Japanese Society of Snow and Ice, Monograph No. 1, pp.1-96.

Appendix

The soil water retention curves of the sediment mixes were computed by using Multi-Fold pF Meter. Fig. A1 shows the relationships between moisture content and matric potential of the soil mass for both sediment mixes 1-6 and 1-7. The relationships between moisture content and matric potential of the soil by using both constitutive relationships of van Genuchten and Brooks and Corey based on curve fitting parameters are also shown in the figures (Fig. A1). By using the curve fitting parameters of soil water retention curve, the values of the soil parameters of the constitutive relationships of van Genuchten were determined as

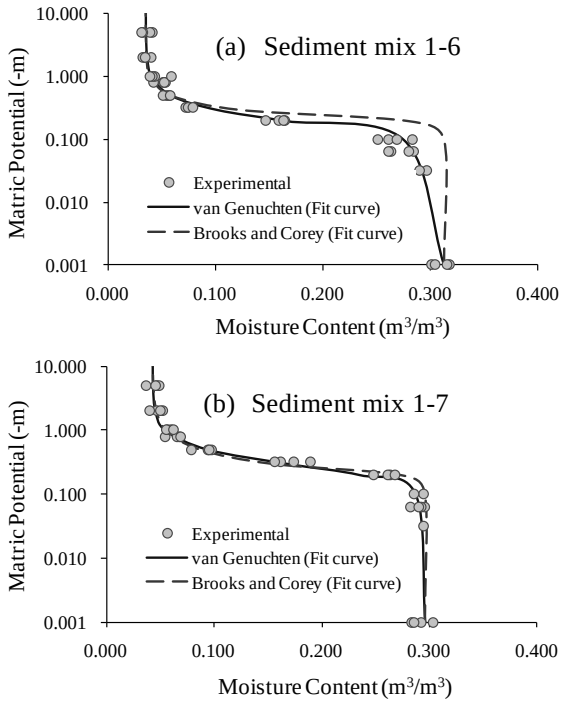

Fig. A1 Relationships between moisture content and matric potential of the soil mass

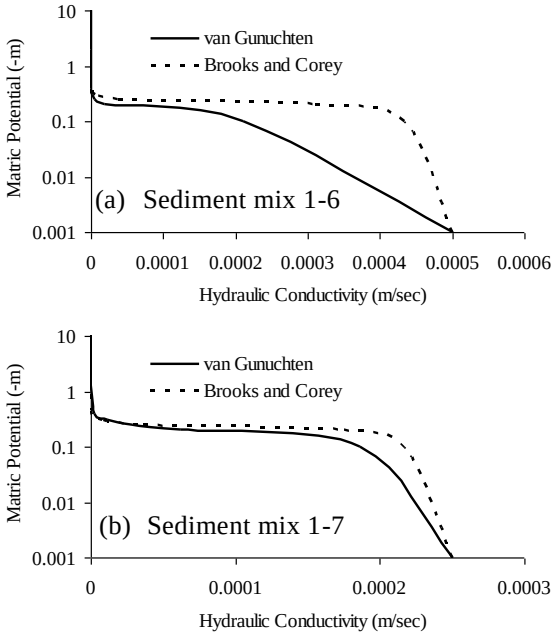

Fig. A2 Comparison and relationships between matric potential and hydraulic conductivity by using van Genuchten and Brooks and Corey relationships

α =6.3, $\eta = 3.1$ and α =4.0, $\eta =$ 3.2 for sediment mixes 1-6 and 1-7, respectively. The values of the soil parameters of the constitutive relationships of Brooks and Corey were determined as λ =2.5, ψ_b =-0.19 and λ =1.8, ψ_b =-0.19 for sediment mixes 1-6 and 1-7, respectively.

The constant head permeability tests were also carried out to determine the saturated hydraulic conductivity of the soil mass. The measured values of the saturated hydraulic conductivity and the saturated moisture content are $K_s = 0.0005 m/\sec$ and $\theta_s = 0.312$ for sediment mix 1-6 and $K_s = 0.00025 m/\sec$ and $\theta_s = 0.296$ for sediment mix 1-7. Fig. A2 shows the relationships between the matric potential and the hydraulic conductivity calculated by using van Genuchten and Brooks and Corey relationships. Fig. A3 shows the relationships between matric potential and hydraulic conductivity based on sediment mixes.

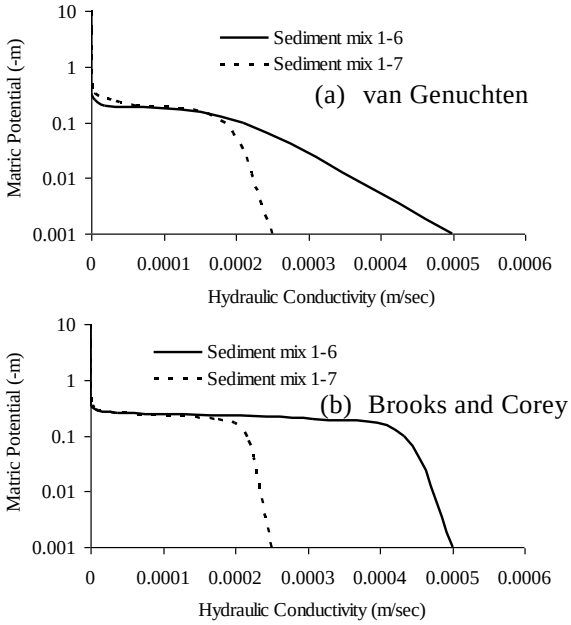

Fig. A3 Relationships between matric potential and hydraulic conductivity based on sediment mixes

ネパール・ロールワリン渓谷における氷河ハザードアセスメントと数値解析による氷河湖決壊洪水の予測

Badri Bhakta SHRESTHA・中川一・川池健司・馬場康之・張浩

要　旨

近年，南アジアのヒマラヤ地域やその他の氷河地帯で，気候変動と氷河の後退に起因する大きな災害が発生している。気候変動の影響で氷河湖は急速に発達・拡大しており，決壊の危険性が指摘されている。氷河湖の決壊は下流域に壊滅的な洪水や災害をもたらす。したがって，気候変動が氷河湖に与える影響を調査し，氷河湖の挙動を把握することが不可欠である。本研究は，ネパール・ヒマラヤのツォ・ロルパ氷河湖での現地調査について報告するとともに，気候変動がツォ・ロルパ氷河湖にもたらす影響について検証を行うものである。ツォ・ロルパ氷河湖はネパールで最も大きく，潜在的危険性の最も高い氷河湖である。浸水・越流によるモレーンダムの決壊が引き起こす氷河湖決壊についての数値解析モデルを構築し，その解析結果を実験により得られた結果と比較した。

キーワード：氷河湖決壊洪水，気候変動，モレーンダム決壊，数値解析，ツォ・ロルパ氷河湖，氷河ハザードアセスメント